Volume 5
Number 23
7 December 2024
Pages 9127–9504

Materials Advances

rsc.li/materials-advances

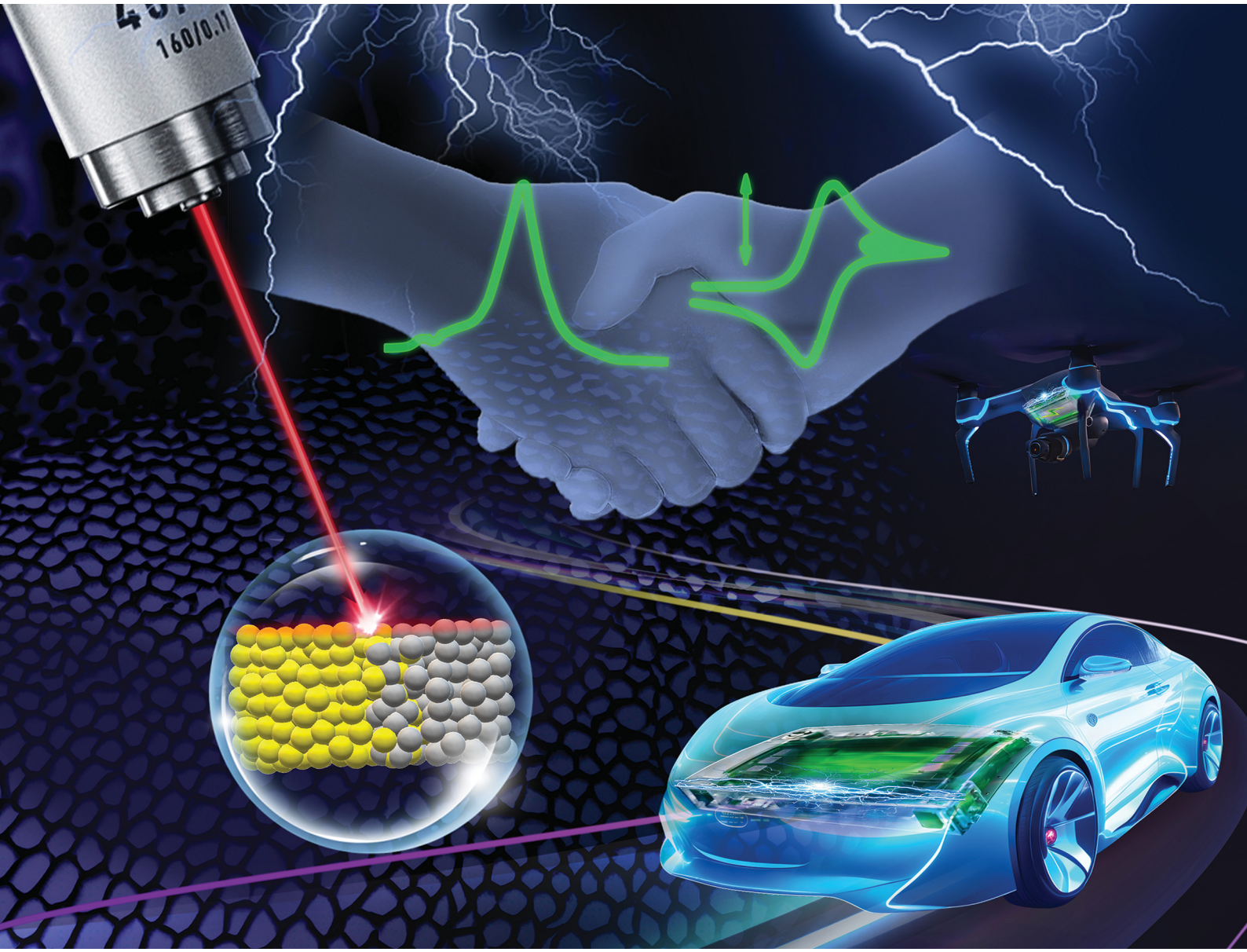

ISSN 2633-5409

ROYAL SOCIETY OF CHEMISTRY

REVIEW ARTICLE
Guang Yang *et al.*
Integrated electro- and chemical characterization of sulfide-based solid-state electrolytes

Materials Advances

ROYAL SOCIETY OF CHEMISTRY

REVIEW

View Article Online
View Journal | View Issue

Cite this: *Mater. Adv.*, 2024, 5, 9138

Integrated electro- and chemical characterization of sulfide-based solid-state electrolytes

Yuanshun Li,[ab] Michelle Lehmann,[a] Lei Cheng,[a] Thomas A Zawodzinski,[ab] Jagjit Nanda[c] and Guang Yang *[a]

Received 15th June 2024,
Accepted 25th September 2024

DOI: 10.1039/d4ma00619d

rsc.li/materials-advances

Sulfide solid-state electrolytes (SSEs) represent a critical advancement towards enabling next-generation lithium metal batteries. However, a profound knowledge gap remains in understanding the structure–property relationships inherent to these sulfide SSEs. Electrochemical assessment and spectroscopic tools, such as Raman spectroscopy, offer bench-top ready, non-invasive, powerful avenues for *operando* and *in situ* analyses. Despite this potential, the integration of these methodologies, particularly for real-time interrogation, is markedly under-investigated. This review endeavors to catalog the use of diverse electrochemical techniques and spectroscopic tools in elucidating the structural and functional nuances of sulfide SSEs. Through the harmonization of these multifaceted evaluation strategies, our objective is to chart a course towards optimized sulfide SSEs, thereby aiding in the development of informed protocols for a deeper comprehension and understanding of the structure–property relationship and interfacial engineered design of solid-state batteries using sulfide-based SSEs.

1. Overview of sulfide solid-state electrolytes: the necessity for multimodal evaluations

Due to the growing interest in sulfide solid-state electrolytes (SSEs) for advanced battery technologies, numerous review papers have thoroughly documented their development. Li *et al.* explored the evolution of sulfide-based composite electrolyte films, emphasizing the function of polymer binders and the associated challenges in optimizing ionic transport and processing methods.[1] Suci *et al.* categorized various sulfide-based electrolytes, focusing on their ionic conductivity and stability while highlighting issues like material scarcity and instability in humid environments.[2] Reddy *et al.* provided insights into sulfide and oxide electrolytes, stressing the impact of synthesis and experimental conditions on their electrochemical performance.[3] Lau *et al.* examined sulfides as alternatives to liquid electrolytes, focusing on their conductivity and processing ease but underscoring challenges like dendrite

[a] *Chemical Sciences Division, Oak Ridge National Laboratory, Oak Ridge, Tennessee 37831, USA. E-mail: yangg@ornl.gov*
[b] *Department of Chemical Engineering, University of Tennessee Knoxville, Knoxville, TN 37966, USA*
[c] *Applied Energy Division, SLAC National Accelerator Laboratory, 2575 Sand Hill Rd, Mailstop 0027, Menlo Park, CA 94025, USA*

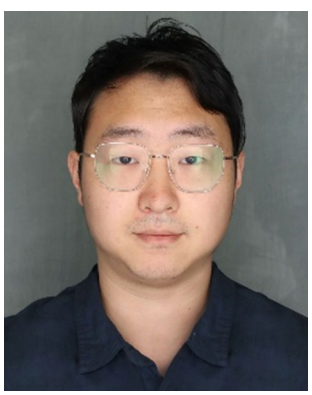

Yuanshun Li

Yuanshun Li is a PhD candidate in Chemical and Biomolecular Engineering at The University of Tennessee, Knoxville. His research focuses on developing electrochemical methods for energy storage devices, particularly sulfide solid-state and zinc slurry air batteries. He is passionate about learning new methods and integrating different characterization practices into understanding interfacial mechanisms in diverse perspectives.

Michelle Lehmann

Dr Michelle Lehmann is a polymer chemist with extensive experience in the synthesis and characterization of various polymer electrolytes. Her expertise has been applied to various applications including flow battery membranes, fuel cell membranes and ionomers, ion-conducting polymers for batteries and binders for cathode/solid-state electrolytes.

suppression.[4] Lee *et al.* addressed scaling issues in sulfide-based batteries, such as binder selection and air stability,[5] while Ren *et al.* further analyzed these challenges, focusing on interfacial instabilities and mass production hurdles.[6] Finally, Su *et al.* summarized recent advances in sulfide electrolytes, focusing on synthesis mechanisms, electrolyte stability, and extending their discussion to high-energy-density all-solid-state batteries.[7]

While previous reviews have provided foundational insights into sulfide SSEs, our review distinctively highlights the integration of Raman spectroscopy with electrochemical methods, offering innovative approaches to overcome the field's most pressing challenges. Our multimodal approach aims to provide a deeper understanding of the mechanisms at play in optimizing sulfide electrolytes. This comprehensive perspective not only looks at improving ionic conductivity and stability, but also investigates how advanced spectroscopic characterization can be combined with electrochemical performance testing to identify and resolve interfacial issues. This approach fills a critical research gap, offering new strategies for enhancing the practical applications and scalability of sulfide-based all-solid-state batteries.

1.1 Sulfide SSE introduction

To address the growing concerns associated with the finite nature of fossil fuels and their carbon dioxide emissions, there is a significant demand for renewable energy storage technologies. Lithium-ion batteries (LIBs) have emerged as the leading solution for energy storage applications, both stationary and in transportation, due to their superior power density, satisfactory energy density, exceptional stability, and outstanding capacity retention. However, traditional LIBs employ organic liquid electrolytes (LEs), which present numerous safety hazards, including flammability and leakage, along with a limited

Lei Cheng

Cheng is the Group Leader of the Energy Storage and Conversion Group at Oak Ridge National Laboratory. Her research focuses on using multiscale computational methods to study material structures, properties, and interfacial reactivities for energy storage applications.

Thomas A Zawodzinski

Dr Thomas A. Zawodzinski is a Governor's Chair in Electrical Energy Storage with a joint appointment at The University of Tennessee, Knoxville and Oak Ridge National Laboratory. His research group focuses on the fundamental science and application of fuel cells, redox flow batteries and metal–air batteries. Prior to this appointment, he was the F. Alex Nason Professor of Engineering at Case, Director of the Case Advanced Power Institute and the Ohio Eminent Scholar in Fuel Cells. He was also the team leader for Fuel Cells in MST-11 at Los Alamos National Laboratory.

Jagjit Nanda

Dr Jagjit Nanda is a Distinguished Scientist and Executive Director of the SLAC-Stanford Battery Research Center. He holds adjunct professorship in Materials Science at Stanford University and is a Scholar at Stanford's Precourt Energy Institute. An internationally renowned expert in battery technologies and energy storage, focusing on advanced chemistries, solid-state, and grid-scale storage, Dr Nanda has authored over 250 journal articles and holds more than 15 patents. His accolades include two R&D 100 awards and fellowships with the Electrochemical Society, Materials Research Society, and National Academy of Inventors.

Guang Yang

Dr Guang Yang is a Battery Material Scientist at Oak Ridge National Laboratory's Energy Storage & Conversion Group. He spearheads several DOE-funded initiatives on advanced battery technologies and sustainable energy conversion, focusing on high-energy solid-state batteries, redox flow batteries, and electrochemical CO_2 conversion. Recognized with the ARPA-E IGNIITE Early Career Award and the UT-Battelle Outstanding Scholarly Output Award, Dr Yang has authored over 80 peer-reviewed publications, two book chapters, and has filed six patents and invention disclosures.

thermal operating range. SSEs serve as an alternative solution, capable of operating across a broad temperature range from −10 °C to 100 °C,[8] mitigating concerns about freezing or boiling of the electrolyte. Over the past decade, many SSEs have been synthesized and implemented in industrial prototypes, including oxide-based, sulfide-based, polymer, and composite materials.[9] Among these, sulfide-based SSEs are particularly effective due to their high ionic conductivity at ambient temperatures, exceeding 1 mS cm^{-1}, comparable to LEs for commercial Li-ion batteries. Besides conductivity aspects, SSEs also possess desirable mechanical properties for room temperature manufacturing purposes.

Sulfide SSEs exhibit enhanced ionic conductivities relative to other SSEs, because of the greater polarizability of sulfur anions compared to oxygen anions,[10] which promotes expedited lithium-ion transport. For example, garnet-type $Li_7La_3Zr_2O_{12}$ (LLZO),[11] an oxide-based SSEs, demonstrates an ionic conductivity of approximately 10^{-4} S cm^{-1}. Lithium phosphorus oxynitride (LIPON), another oxide-based SSE, has a markedly lower ionic conductivity, approximately 10^{-6} S cm^{-1}, yet it is prevalently utilized in thin-film battery applications due to its stability and compatibility with lithium metal anodes.[11] The field of solid-state battery research has seen a surge of activity following the discovery of a new solid-state electrolyte known as $Li_{10}GeP_2S_{12}$ (LGPS). This material has demonstrated an outstanding ionic conductivity, measured to be 1.2×10^{-2} S cm^{-1} in 2011.[12] Tatsumisago *et al.* reported a glass ceramic $Li_7P_3S_{11}$ with a high conductivity of 1.1×10^{-2} S cm^{-1} in 2014.[13] Subsequently, Kato *et al.* reported a LGPS structure derivative $Li_{9.54}Si_{1.74}P_{1.44}S_{11.7}Cl_{0.3}$, which had the highest conductivity of 2.5×10^{-2} S cm^{-1} in 2016.[14]

Li argyrodite compounds, such as Li_6PS_5Cl, have emerged as the preeminent material for sulfide SSEs in all-solid-state batteries, owing to their facile synthesis and remarkable ionic conductivity, reaching up to 2.4×10^{-2} S cm^{-1}.[8] Despite the high ionic conductivity that facilitates rapid charge–discharge cycles in all-solid-state batteries, these materials face several critical challenges, including complexities in synthesis, structural modifications during processing, inherent moisture sensitivity, a constrained electrochemical stability window, and issues pertaining to the solid electrolyte interphase.[9,10,15–17] To overcome these challenges, we believe that evaluations on the SSEs combining the chemical and electrochemical means are essential.

1.1.1 Introduction of different chemical characterization. Many chemical characterization tools can help with interpreting sulfide SSE's chemistry. X-ray diffraction (XRD) is the go-to method for elucidating the crystalline structure of sulfide SSEs. By analyzing the diffraction patterns, we can determine the phase composition, identify any secondary phases, and assess the degree of crystallinity to analyze the material's performance and stability. X-ray photoelectron spectroscopy (XPS) delves into the surface chemistry (usually nano resolution), offering a detailed view of elemental composition and oxidation states present on the SSE surface. This is particularly important for examining interfacial reactions and the formation of passivation layers.

X-ray absorption near edge structure (XANES) provides another layer of detail, particularly when probing the sulfur K-edge, allowing us to investigate the local electronic structure and oxidation states of sulfur within the SSE matrix. This allows us to identify the existence of side products, for example elemental sulfur. X-ray computed tomography (XCT) offers a three-dimensional perspective, visualizing the internal microstructure of the SSEs.

Infrared (IR) spectroscopy complements these techniques by focusing on the molecular vibrations within the SSE, providing insights into the bonding environments of elements such as sulfur and the presence of specific functional groups. This can be particularly useful for identifying subtle changes in the chemical structure that might not be apparent through other methods. Additionally, nuclear magnetic resonance (NMR), especially when using isotopes like Li_7 and sulfur-related, offers a powerful tool to probe the diffusion of lithium ions.

However, many of these characterization tools usually only allow *ex situ* measurements because of several major challenges. First, some advanced spectroscopy tools such as XRD, XPS, XANES, and XCT have strong laser power which causes irreversible damage to samples after experimental measurement. Second, sulfide SSEs are air-sensitive, so a special house-designed sealed sample holder or cell mold is required. Furthermore, the sulfide compounds can contaminate instruments, often requiring a sulfide-dedicated instrument, which can be very challenging for many researchers.

Raman spectroscopy was found to be particularly effective in monitoring structural changes in sulfide SSEs during battery electrochemical testing, and it is a benchtop instrument that is broadly available.

Usually, electrochemical methods are considered noninvasive. However, most of the postmortem chemical evaluation methods require cell disassembly. Therefore, the development of a nondestructive chemical evaluation method, preferably aligned with the electrochemical method, becomes necessary. Our team and others have demonstrated that in *operando* Raman spectroscopy and imaging, facilitated by machine learning analysis, is effective in probing the sulfide SSE structure,[18] chemistry after solvent processing,[19] and interface during SSB operation.[20–22] Employing this integrated approach can reveal the fundamental structure–property relationships of charge–discharge processes for sulfide SSEs to foresee failure mechanisms. Despite the growing number of studies on sulfide solid-state batteries (SSBs), there remains a notable gap in the review literature that provides an overview of commonly used electrochemical methods, and the integration of *in situ* Raman spectroscopy for SSB evaluations. Fig. 1a presents a summary of the number of review articles published in the field of sulfide SSBs, identified through keyword searches on the Web of Science (WOS) database. Out of 169 SSB-related review papers, only 14 discuss *in situ* or *operando* characterization techniques. Among these, only one addresses the use of Raman spectroscopy in sulfur-based batteries. As noted in Fig. 1b, only two research papers mentioned Raman mapping with electrochemistry in sulfide SSBs.

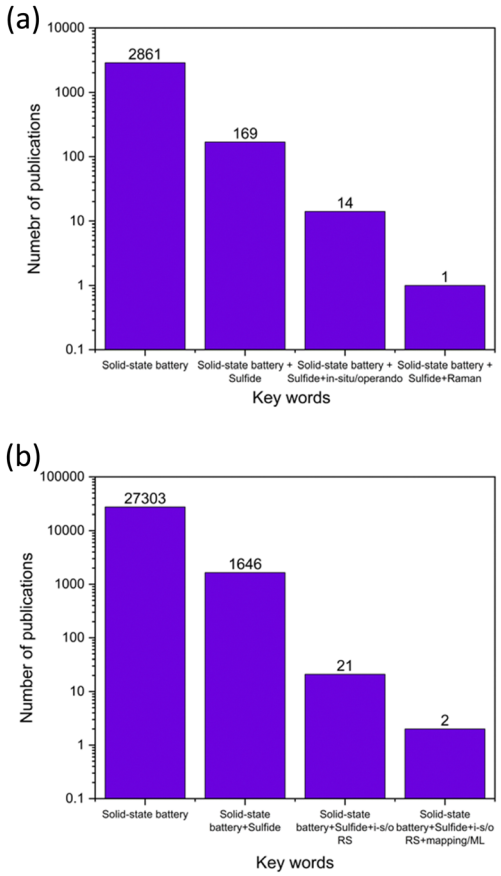

Fig. 1 Comparison of publication counts *vs.* keywords for (a) review papers and (b) all papers, sourced from Web of Science Database (1961–2024).

This review seeks to bridge the gap by offering a comprehensive view that integrates traditional electrochemical techniques with *in situ* Raman spectroscopy in the field of sulfide SSBs. Our goal is to confront pressing interfacial challenges and catalyze new research directions in the field.

1.2 Current challenges requiring multimodal characterization and research trends

1.2.1 Informed sulfide SSE fabrication. Due to scope limitations, we focus specifically on the combination of multiple electrochemical methods and chemical techniques provided by Raman spectroscopy for a comprehensive multimodal evaluation.

The fabrication of sulfide SSEs, including mechanochemical means, such as ball-milling, and wet chemical processes, such as solvent-mediated synthesis,[18] which plays a crucial role in influencing the material's structure and inherent properties. It is desired to apply a knowledge-based approach to producing sulfide SSEs, using specific information and techniques to optimize the process and the performance of the resulting materials. Therefore, it is important to employ multimodal analytical techniques to probe the structure–property relationships and their subsequent impact on performance post-fabrication. In this section, we introduce the traditional methods for synthesizing sulfide SSEs first and then present established and effective electro and chemical techniques for the characterization and evaluations of emerging sulfide SSEs.

The conventional fabrication of SSEs necessitates high-temperature solid-state synthesis, which involves thermally induced bond-breaking and requires substantial energy input, thus constraining scalability due to a time-consuming annealing step. An alternative mechanochemical technique, commonly referred to as "ball-milling," has been developed for the synthesis of SSEs. This method utilizes mechanical forces to manipulate material size and crystal defect formation in a non-equilibrium state.[23] Notably, the superionic conductor argyrodite (Li_6PS_5X, X = Cl, Br, I) has been effectively synthesized *via* ball milling, substantially reducing crystallization time compared to traditional solid-state methods.[23] The efficiency of ball milling and the resultant product quality are influenced by three critical parameters: milling media-to-sample ratio, milling speed, and milling time. These variables govern the specific reaction yield, surface area, particle size, and byproducts formation. Yu *et al.* reported the Li ion mobility of Li_6PS_5Br is strongly affected by the milling time over different crystallographic sites.[24] However, comprehensive studies to optimize the ball milling parameters for the crystal structure and morphological characteristics of SSEs have not been extensively reported.

The integration of solution-assisted synthesis with ball milling represents a compelling approach for the fabrication of SSEs. This method involves the homogeneous dispersion or suspension of SSE precursors in a carefully selected solvent, which must solubilize the precursors without inducing the formation of undesirable byproducts. Ethanol and *N*-methyl formamide (NMF) are effective solvents for Li_2S and LiX; however, they may adversely react with and decompose P_4S_{10}.[25,26] Conversely, tetrahydrofuran (THF) is unsuitable for argyrodite synthesis due to the reactants' insolubility in this medium. To address these challenges, the synthesis methodology has been refined by initially forming Li_3PS_4, followed by the incorporation of additional Li_2S and LiX. However, the chemistry behind solvent-assisted processes within the reaction pathways remains largely unelucidated. Therefore, multimodal assessments are necessary to understand the effects of different fabrication methods on newly synthesized SSEs' chemical and electrochemical properties. Raman spectroscopy is widely applied to investigate the structural and chemical attributes of fresh SSEs. For example, pristine LPSCl has been reported that has an almost centered 425 cm^{-1} Raman shift peak indicating a PS_4^{3-} tetrahedra structure,[27] as presented in Fig. 2. However this P–S stretching bond can shift to 440 cm^{-1} in LGPS,[28] and 418 cm^{-1} in β-Li_3PS_4.[29]

The reason behind this shift is due to its underlying crystalline structure. For example, the compound Li_6PS_5Cl adopts a crystalline structure within the cubic $\bar{F}43m$ space group. This structure is characterized by a Li_6PS_5 framework interspersed with four clusters of Cl_2. Within each of these clusters, each Cl^- ion is surrounded in a 12-coordinate geometry by surrounding atoms. Within the overarching Li_6PS_5 scaffold, each Li^+ ion is arranged in a trigonal planar configuration, coordinating with three S^{2-} ions. The Li–S bonds vary in length, featuring one shorter bond at 2.33 Å and two longer bonds at 2.42 Å. Phosphorus (P^{5+}) is tetrahedrally

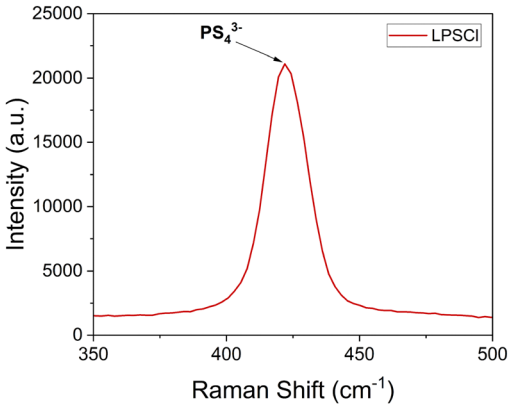

Fig. 2 An example of a Raman single spectra for pristine LPSCl shows a P–S stretching bond at around a Raman shift of 425 cm^{-1}.

coordinated, linking symmetrically to four identical S^{2-} ions, each at a bond length of 2.06 Å. Sulfur (S^{2-}) manifests in two distinct coordination environments. In the first, a sulfur ion is surrounded by six Li^+ ions, forming a corner-sharing SLi_6 octahedron. In the second environment, a sulfur ion bonds with three equivalent Li^+ ions and one P^{5+} ion to create a SLi_3P tetrahedron. This tetrahedron shares corners with three SLi_6 octahedra and six additional SLi_3P tetrahedra. The structure features octahedral tilt angles of 54°, which indicates the degree of spatial rotation within these octahedra. The most featured Raman peak is centered around 425 cm^{-1}, representing the P–S stretching mode for the PS_4^{3-} tetrahedra.

Concurrently, electrochemical impedance spectroscopy (EIS) measures bulk ionic conductivity and electrode/SSE interfacial resistance, and linear sweep voltammetry (LSV) delineates the electrochemical stability window, capturing the oxidation and reduction potentials. These parameters, obtained through multimodal evaluation, serve as essential baselines that can further be applied in molecular dynamics (MD), density functional theory (DFT) calculations, and machine learning (ML) to predict potentially useful new SSEs.[30] Conversely, while computational methods provide valuable insights into the design of materials in crystalline phases, predicting synthesis and the impact of processing on material performance remains challenging. To bridge the gap between multimodal characterization techniques and the structure–property relationships in SSEs, the integration of these techniques enables a deeper understanding of how synthesis parameters influence sulfide SSE properties. By correlating the structural and chemical data obtained from Raman spectroscopy, EIS, and LSV with the observed electrochemical performance, we can inform and optimize synthesis processes to tailor sulfide SSEs with desirable properties. This informed approach not only refines current methodologies but also guides the development of new materials with enhanced performance characteristics.

1.2.2 Sulfide SSE and SSB manufacturing. Manufacturing sulfide SSEs and SSBs includes a sequence of dry and wet chemical processes, such as slurry preparation, tape casting, calendaring, and cell assembly.[19] Throughout these stages, interactions between the solid electrolyte, solvents, and binders may induce chemical and structural transformations in the sulfide SSE, potentially altering its characteristics and performance. Hence, it is critical to perform on-the-fly assessments of the SSE's chemistry and structure during the manufacturing workflow. In the following content, we will detail the evolution of cell design principles aligned with the industrial supply chain and exhibit the cutting-edge developments in sulfide-based SSBs. The evolution of designs should be guided scientifically through systematic studies – an integrated approach combining electrochemistry and chemistry. To achieve this, key SSB manufacturing parameters that are critical to evaluate with both multiple electrochemical and chemical techniques should be evaluated.

As aforementioned in Section 1.2.1, interactions between solvents and sulfide SSEs may alter their structures. Similarly, solvent processing during manufacturing plays a critical role in determining the structure stability of sulfide SSEs. Methods such as tape casting involve solvents that can introduce structural defects if not controlled properly. These defects can affect the ionic conductivity and mechanical properties of the SSEs, thereby affecting the structural integrity of the thin SSE films.[31] Recent advances were made in Zhao *et al.*'s group, as they systematically studied the solvent effects in processing LPSCl membranes.[32] This study integrated XRD, XPS, Raman, and EIS as a 'chemistry checker' to inform whether as-made films experienced degradation from structural change in various solvents. There is no doubt that this multimodal approach can strengthen the chemical evidence for processing science. Usually, a single characterization cannot provide convincing scientific findings, and requires back up supporting evidence provided using other characterization tools. For example, Delnick *et al.* reported that Raman spectroscopy and XPS are co-used to determine the chemical structure of several Li–P–S ternary compounds.[18] This is because Raman spectroscopy alone is insufficient to reveal this structure, due to a lack of distinguished peaks of some of the S ternary compounds.

Another factor during the sulfide SSE and cell manufacturing is the processing environment. The environmental conditions are crucial for sulfide SSE stability and performance. Shirley Meng *et al.* comprehensively examined LPSCl stability under different operating conditions,[27] such as exposure to air, and exposure to water followed by heat treatment. In this paper, they found pristine LPSCl has PS_4^{3-} at a Raman shift to exactly 425.2 cm^{-1}, and any exposure can cause the peak position to shift which indicates a local structural change. Notably, the air exposed LPSCl had a peak Raman shift all the way to 418 cm^{-1}, suggesting significant side product degradation occurs. To unveil the chemistry, FTIR was further applied to the air exposed sample and revealed that the C=O carbonate bond and O–H stretching suddenly appeared at frequencies of 3000–3500 cm^{-1} and 1427 cm^{-1}. This indicates LPSCl experienced hydration and reaction with CO_2. Furthermore, air exposure of LPSCl resulted in a loss of at least one order of magnitude of ionic conductivity as measured by EIS, even with 550 °C heat treatment. Correlating ionic conductivity with local structure can also be found in H. Muramatsu *et al.*'s report.[33] This study utilizes solid-state NMR to examine the structure and

dynamics of Li_2S–P_2S_5 based solid electrolytes, providing insights into the ionic conduction mechanisms in SSBs. Other techniques were also frequently reported to study the interfacial stability and reactions in sulfide SSBs. For example, K. Kang *et al.* discusses the use of XPS and TEM to analyze the native defects of LGPS.[34] Multimodal characterization is beneficial in bridging the gap between fundamental and manufacturing science.

The scope of this mini-review will focus on combining an electrochemical method and Raman spectroscopy to study sulfide SSEs.

Raman spectroscopy can be used in controlled environments such as dry rooms or gloveboxes to prevent moisture and air exposure, which can degrade the materials, to explore the structure of the sulfide SSEs. Meanwhile, the properties of the sulfide SSE exposed to a specific environment can be evaluated by multiple electrochemical means.[35] Surface coatings, such as Al_2O_3, $LiNbO_3$, and short chain polymers, create a barrier that prevents the sulfide SSE particle being exposed to air.[36,37] Raman spectroscopy can monitor these coatings' effectiveness by detecting characteristic Raman shifts which indicates degradation products like H_2S.

In-line Raman spectroscopy can provide real-time monitoring for quality control during the manufacturing of sulfide SSEs. This technique allows manufacturers to observe the chemical composition and structural changes in real-time, ensuring that the final product meets the desired specifications. Implementing an in-line Raman systems helps detect and correct issues promptly, optimizing the manufacturing process.

When manufacturing sulfide-based SSBs, the compatibility of the electrode and the SSE is vital for whole-cell integration. The multimodal approach helps reveal the chemical and mechanical stresses at these interfaces, providing insights into designing more stable and efficient SSBs.

Traditionally, the lithium anode thickness was thicker than the combined solid electrolyte and cathode layers, based on the design that maximizing lithium content would enhance the theoretical capacity and energy density of the cell. Nevertheless, such designs for thick lithium anodes have encountered significant challenges, including substantial volume changes during electrochemical cycling, the formation of lithium dendrites, and an unfavorable trade-off between energy density and the intrinsic weight and volume of lithium. Consequently, contemporary design philosophy has shifted towards the 'anode-free' approach. This approach completely removes the lithium metal anode, choosing instead to directly deposit solid-state electrolytes onto the current collector. This strategy must have lithium included within the cathode composite itself, potentially through alloys with nickel manganese cobalt oxide (NMC), sulfur, or nitrogen-doped materials, to ensure the presence of lithium for the initial charging process. Fig. 3 shows the developments of components and designs to increase the energy density.

Lee and colleagues at Samsung have developed a prototype pouch cell with a capacity of 0.6 Ah, realizing an energy density exceeding 900 W h L^{-1} and maintaining 99.8% CE across 1000 cycles, which marks the state of the art performance in all solid-state batteries.[39] This was accomplished by employing an Ag–C composite anode in a lithium-free anode configuration. The detailed manufacturing processes of this advanced pouch cell were revealed, noting the application of a processing pressure of 490 MPa and a stack pressure between 2–4 MPa. This information is vital given that all-solid-state battery technology is acutely pressure-dependent, contrasting with conventional liquid electrolyte lithium-ion batteries where pressure sensitivity is less critical. Meng *et al.* also investigated the impact of pressure on the performance of SSBs, offering practical insights on the significance of pressure in these systems.[40] However, there is a gap in understanding how these manufacturing parameters, for example, cell processing and stack pressures, affect sulfide electrolyte lattice structural defects, parasitic side products, and chemical compositions over cycling. Raman spectroscopy and imaging have the great potential to decipher the SSE structure with different processing conditions. For

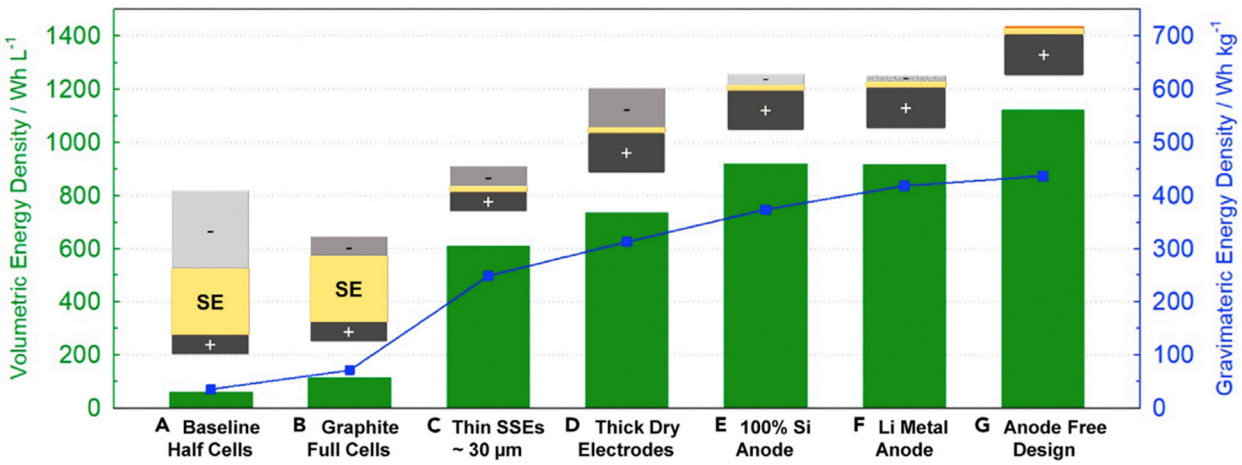

Fig. 3 Calculation of the energy density of ASSBs as a function of cell parameters, highlighting the advanced research progress towards practical scalable manufacture. Achievements include (B) graphite anode, (C) thin SSEs ~30 μm, (D) thick cathode, (E) Si anode, (F) thin lithium metal, and (G) state of art anode free design. Reproduced from ref. 38 with permission from Elsevier, copyright 2022.

example, we have shown that when processed by different solvents during slurry casting, the argyrodite sulfide SSE has varied stability against a lithium metal anode.[31]

The next section will discuss this core approach that intrinsically catalyzed the new direction, cross-talk between electro- and chemical characterization.

2. Evaluating SSEs: conventional approaches and *in situ* Raman spectroscopy (*is*-RS)

The advantages of electrochemical methods are beneficial to quantify sulfide SSB performances. However, they lack a fundamental understanding of the underlying chemistry. Raman spectroscopy can resolve this issue by directly imaging the structural difference. For example, J. Lim performed full sulfide SSB galvanostatic cycling in the first cycle and the initial poor coulombic efficiency is obvious.[41] Raman mapping revealed the degradation is attributed to the formation of (CH_3)–S, highlighting the importance of choosing an appropriate carbon ratio. S. Liatard performed a direct dry room exposure study on the sulfide SSE.[42] Both EIS and galvanostatic cycling clearly show LPSCl outperforms $Li_7P_3S_{11}$ with higher ionic conductivity and optimal capacity both before and after exposure. The reason for the higher performance of LPSCl was further confirmed from the Raman spectrum. It shows a more centered P–S stretching bond and no detected deformation product – $P_2S_7^{4-}$ in LPSCl. X. Li *et al.* reported a nanolayer coating of $LiCoO_2$ (LCO) on a high nickel NMC cathode significantly enhances cycling stability, registered at 585 cycles with 80% capacity retention.[43] dQ/dV analysis also indicates that the H2–H3 phase was mitigated with an LCO coated cathode during cycling. To understand what exactly is happening in the cathode electrolyte interphase, Raman spectroscopy revealed that a new peak at 1441 cm^{-1} appeared for the uncoated the NMC but couldn't be seen for the LCO-coated NMC in the cycled samples. This peak is assigned to phosphate–sulfate like species and indicates the LCO coating effectively suppressed this undesired species, which improves cell performance.

As pre-described evidence, we demonstrate the strong necessity to combine electrochemical methods with Raman spectroscopy. In the following context, we will detail the general application of each electrochemical method and Raman spectroscopy. Furthermore, we will explore their limitations and include comprehensive discussion of the importance of multimodal characterization in sulfide SSBs.

SSEs present many interfacial challenges that necessitate comprehensive evaluation of their fundamental properties prior to integration into full-cell configurations. Critical parameters such as ionic conductivity, electrochemical stability window, and electrode–electrolyte interfacial stability must be assessed. Established electrochemical techniques—such as EIS, linear sweep voltammetry/cyclic voltammetry (LSV/CV), and galvanostatic cycling (GC)—are utilized to gauge these essential characteristics within a half cell configuration but in different designs. EIS typically uses two pieces of stainless steel (SS) as blocking electrodes, whereas LSV/CV employs lithium metal as the working electrode, with either SS or platinum as the counter electrode. In GC, it is common to use two lithium foils or plates as electrodes.

Upon demonstrating satisfactory performance in half cell tests, including enhanced stability and conductivity, SSEs are then incorporated into full cells to evaluate overall battery performance metrics such as capacity retention across various C-rates, temperatures, pressures, and cathode active material (CAM) loadings.[44] Interfacial resistances and Li^+ diffusion coefficients are further discerned *via* EIS and a galvanostatic intermittent titration technique (GITT) within the full cell to elucidate the mechanisms underlying battery failure.[45] Additionally, *in situ*/*operando* Raman spectroscopy serves as an interdisciplinary method to monitor real-time structural and compositional changes at the interphases, correlating these observations with performance degradation.[46] In the following paragraphs, conventional electrochemical methods in this field are summarized and discussed within their key applications.

2.1 EIS: quantify ionic conductivity and interfacial resistance

In the field of energy storage, the ionic conductivity of solid electrolytes is usually quantified through EIS. EIS employs an alternating current (AC) impedance technique where a potential of small amplitude, typically between 5 to 10 mV, is applied while scanning frequencies from 1 MHz to 10 mHz. The impedance spectrum is commonly visualized using a Nyquist plot, which facilitates the interpretation of resistances based on an equivalent circuit model. The ionic conductivity of SSEs is measured in a symmetrical cell configuration utilizing two 'blocking electrodes' (*e.g.*, stainless steel), which do not undergo faradaic reactions.[47] In a 'fresh' cell, the Nyquist plot typically exhibits a linear response, with the intersection on the real axis indicating the total resistance of the SSE. This resistance is converted into conductivity using a straightforward equation.[47] Occasionally, a Nyquist plot may reveal a semicircle in the high-frequency domain, indicative of grain boundary resistance.[45] Thus, EIS serves as an essential and unequivocal method for quantifying the ionic conductivity of SSEs. However, studies probing the interfacial resistance between electrodes and SSE *via* EIS during active discharge–charge cycles are lacking, representing a critical knowledge gap in transitioning from an understanding of solid electrolyte performance in half-cells to full-cell applications.

Besides this, the limitation of EIS in determining either a solid electrolyte's conductivity or interfacial resistance originates from its complexity in interpretation. Specifically, in solid-state batteries, the electrode and electrolyte interfaces are often more complex compared to those in liquid electrolyte systems. This complexity arises from the solid nature of the electrolyte and the potentially diverse interface phenomena, such as interfacial chemical reactions and mechanical stress effects. The use of equivalent circuit models to interpret EIS data can be particularly limiting here, as these models may not accurately capture the intricate physicochemical processes

occurring at these interfaces. For example, the increase in interfacial resistance during SSB operation may be due to the loss of solid–solid contact, the generation of a passive interface, or both. However, EIS fails to discern the exact reason for the increase in interfacial resistance.

On the other hand, solid state batteries may experience overlapping impendence which corresponds to different physicochemical processes. Thus, separating different interphases and bulk conductivity can be very challenging to achieve due to dynamic processes and complicated systems. Systematic standardization has not yet been established for application in the solid state battery research community. In the following context, we try to pinpoint some appealing examples to present how EIS is applied to study different systems, possible interpretation, and a potential strategy to overcome this limitation.

EIS is instrumental for quantifying interfacial resistances at varying states of charge (SOC) in full cells. Zhang *et al.* utilized EIS to analyze resistance contributions throughout galvanostatic charge–discharge cycles in an $In_xLi|LGPS|LiCoO_2$ cell,[48] as presented in Fig. 4. They interpreted impedance spectra using a three-element equivalent circuit model, attributing the high-frequency semicircle to grain boundary resistance, the medium-frequency semicircle to cathode–SE interfacial resistance, and the low-frequency semicircle to anode–SE interfacial resistance. Additionally, bulk or Warburg resistances were identified at the high and low boundaries of the frequency spectrum in Nyquist plots. During charging, the In/LGPS resistance remained relatively constant, whereas the $LiCoO_2$/LGPS resistance significantly increased with rising potential, suggesting possible factors such as crack formation, volume changes, or accumulation of side products leading to increased interfacial resistance as SOC increased.

On the other hand, during discharging, the In/LGPS interfacial resistance increased when the discharge capacity exceeded 50%, while the $LiCoO_2$/LGPS resistance was nearly unaffected. The increasing anode/SE resistance during discharging correlated with the depletion of Li from the Li_xIn alloy.[49] Furthermore, bulk and grain boundary resistances were observed to remain constant across different SOC, resulting of the intrinsic stability of the material itself. This methodology elucidates the contributors to resistance and loss during galvanostatic cycling, providing quantitative electrochemical insights into battery failure mechanisms. However, its interpretation regarding how resistances are assigned still lacks direct supporting evidence. This suggests further *in situ* characterization methods, such as *in situ*/*operando*

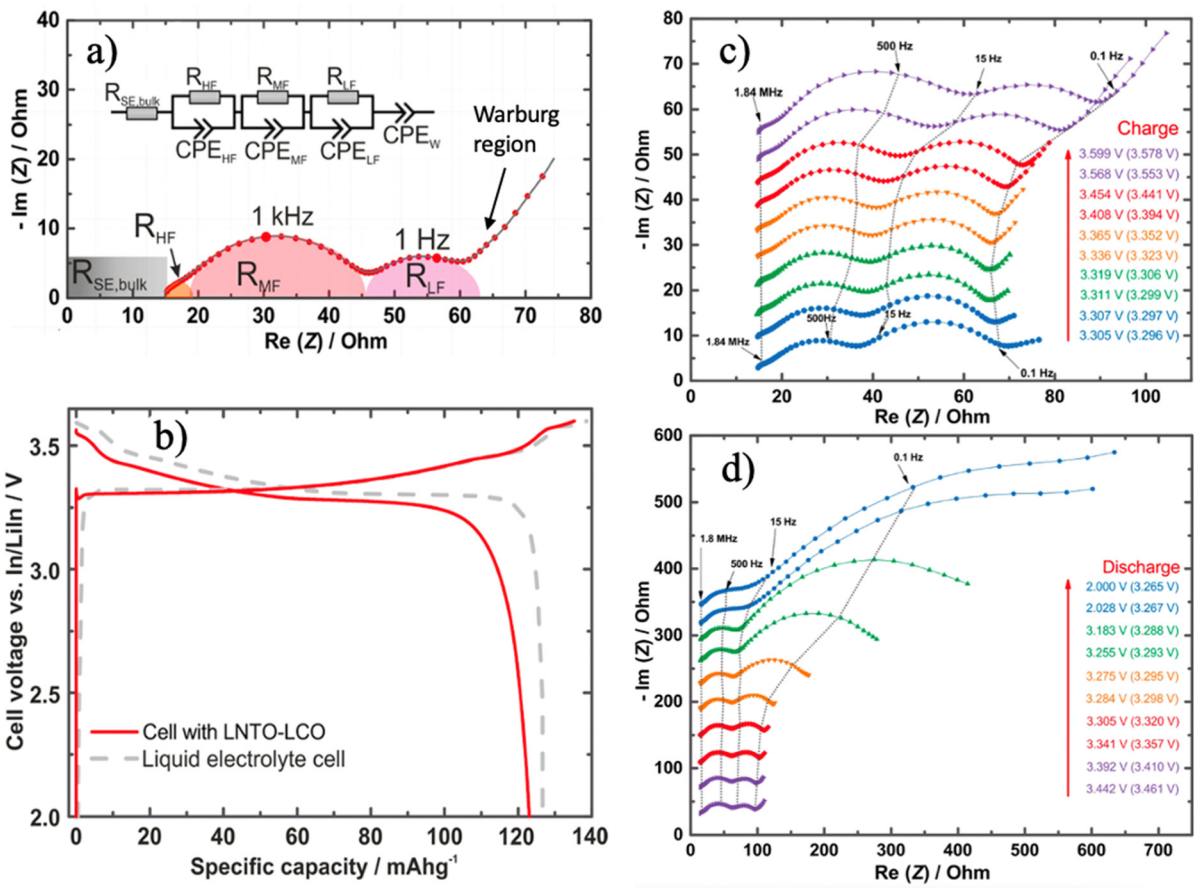

Fig. 4 (a) EIS Nyquist plot with equivalent circuit model simulation to assign a different frequency range to specific resistances; (b) a comparison of LNTO–LCO and liquid electrolyte in the initial galvanostatic charging–discharging profile; SOC dependent Nyquist plot at (c) charging and (d) discharging to highlight the dynamic change of interfacial resistances under different scenarios. Reproduced from ref. 48 with permission from American Chemical Society, copyright 2017.

Raman, X-ray diffraction (XRD), and scanning electron microscopy (SEM) are critically urgent to link chemical and mechanistic interphase observations to a specific frequency of range impendence.

From a chemistry perspective, activation energy is used to describe the mobility of Li-ions through the solid electrolyte interface (SEI), which is related to lithium ion hopping between sites and is quantified through temperature dependent EIS and calculated by the Arrhenius equation as follows:[50]

$$\sigma = A\exp(E_a/kT)$$

where σ is the ionic conductivity, A is the proportional constant, E_a is the activation energy, k is the Boltzmann constant, and T is the absolute temperature. Keefe *et al.* conducted EIS measurements that were temperature-dependent on lithium-ion batteries,[51] as depicted in Fig. 5(a). To clearly present E_a, the R_{ct} is plotted against $1/T$ in log scale as shown in Fig. 5(b). It turns out the slope of the curve directly reflects the magnitude of E_a.

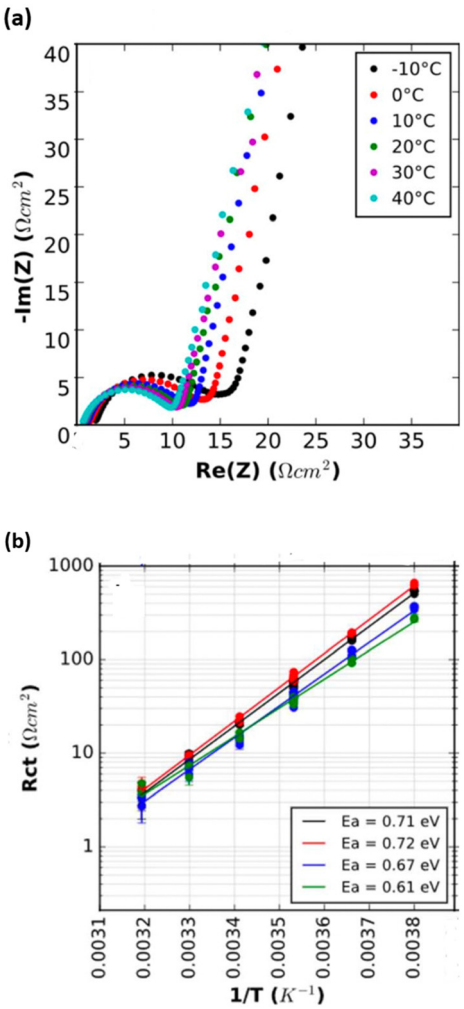

Fig. 5 (a) Temperature dependent Nyquist plot in positive blocking electrode symmetric cells; (b) charge transfer resistance was plotted against the reciprocal of temperature in log scale under positive symmetric cells. (Inset lists the activation energy values of each curve). Reproduced from ref. 51 with permission from The Electrochemical Society, copyright 2019.

In terms of structure, some sulfide SSE types have ionic conductivity comparable to that of liquid electrolytes. For example, experiments show that argyrodite SSE, Li_6PS_5X (X = Cl, Br and I) have the same crystallographic structures (space group $F\bar{4}3m$) as Li_7PS_6 and the ionic conductivity of Li_6PS_5Cl and Li_6PS_5Br at room temperature is high enough to be considered for battery technology.[52] Halogen disorder is believed to be responsible for the high room temperature ionic conductivity as calculations have suggested that extra halogens and Li-vacancies result in higher conductivities.[53] These structures can be probed by Raman spectroscopy. For example, the PS_4^{3-} tetrahedral has a featured band at around 425 cm^{-1}, and this peak can shift upon local chemical environment change resulted from the structural change.[54]

2.2 LSV/CV: determine the electrochemical window of the sulfide SE

In addition to ionic conductivity, the quantification of the electrochemical stability window (ESW) is essential prior to full-cell assessments. ESW delineates the stable potential range for SSEs, establishing the requisite operational boundaries for safe cell cycling and preventing electrolyte decomposition. Linear sweep voltammetry (LSV)[55–57] and cyclic voltammetry (CV)[40,58–61] are employed to determine the ESW of SSEs using a two-electrode setup, typically Li/stainless steel. LSV conducts a unidirectional potential scan, whereas CV reverses the scan back to the initial potential. The Viallet group used CV on a series of halide substituted argyrodite, Li_5PS_6X (X = Cl, Br, I).[62] It shows they are electrochemically stable up to 5 V against Li metal. $Li_{6.1}Ga_{0.05}P_{0.95}S_5Cl$, a Ga substitution argyrodite, further improves their electrochemical stability against Li metal as evidenced in CV.[60] J. Yi *et al.* confirms increasing loading of PEO in LPSCl–PEO3–LiTFSI improves the interfacial stability by LSV.[63] S. Luo *et al.* further employed LSV to explore the electrochemical stability of modified LPSCl through oxygen substitution and adding PEO. Both strategies can significantly stabilize the Li/SE interphase as evidenced by the diminishing oxidation peak.[64] LSV and CV are well-established techniques and widely applied to describe the electrochemical stability in the theoretically low ESW of sulfide electrolytes.

Both LSV and CV possess inherent limitations, notably the tendency to overestimate the onset potential at an arbitrarily chosen threshold current density, *e.g.*, 0.1 mA cm^{-2}. Efforts to mitigate this involve reducing the scan rate to below 0.1 V s^{-1}. However, the onset potential may still be overestimated due to suboptimal contact and consequently low electrical conductivity between the solid electrolyte and the electrode.[65] In contrast, with liquid electrolytes, several challenges affecting the validity of CV are resolvable by: (1) enhanced contact between the electrolyte and electrode; (2) the use of a three-electrode setup, which is more conducive to accurate measurements. Therefore, CV analysis in solid electrolytes requires cautious control of experimental conditions. For example, applying higher external pressure can improve the contact between the SE and electrode, yielding a more reliable estimation of the onset potential.

Other potential limitations are observed when applying CV/LSV in both modeling and experimental aspects. For example, the finiteness of diffusion and the kinetics of electrode reactions can complicate the interpretation of voltammetry data, especially in nanoscale processes.[66] At different scan rates, the size of the diffusion layer and the time taken to record the scan can vary experimentally, leading to different current responses. This dependency on scan rate can obscure the understanding of the underlying electrochemical processes and requires careful calibration and interpretation. Schmickler *et al.* reported that quasi-reversible or irreversible electron transfer reactions occur when electron transfer processes are slow relative to the voltage scan rate.[67] This results in an inaccurate current peak position being used to interpret the kinetics of reactions. We believe a standardization protocol to evaluate the electrochemical stability window of sulfide SSEs by CV/LSV must be established in the near future.

On the other hand, it is known that sulfide electrolytes tend to be oxidized when operating at a higher threshold potential. This resulting structure change and decomposition product can be probed through Raman spectroscopy.[68] J. Zhang *et al.*[69] designed a house-made *in situ* Raman cell to elucidate the LPSCl/NMC interphase during CV measurements. In the first CV scans in both positive and negative sweep, two peaks denoted as 418 cm^{-1} and 425 cm^{-1} are observed, and there is no third peak captured. It is believed that these two peaks are assigned to PS_4^{3-} (*ortho*-thiophosphate) in a different vibrational mode. No obvious signal shows a conversion from PS_4^{3-} to $P_2S_6^{4-}$ (at 410 cm^{-1}) or $P_2S_7^{4-}$ (at 390 cm^{-1}). This indicates no decomposition occurs at this LPSCl/NMC interphase in the first CV cycle. Conversely, Gewirth's group[70] observed a strong peak at 411 cm^{-1}, denoted as $P_2S_6^{4-}$, and other 'deformation' peaks at 178 cm^{-1} and 272 cm^{-1} for the $Li_7P_3S_{11}$(LPS)/Au interphase during a negative sweep. As a result, Raman spectroscopy can bring critical insights of chemical structure in a dynamic potential sweeping process.

2.3 Galvanostatic cycling: to determine the capacity retention capability

Galvanostatic cycling (GC) is a technique wherein a constant current density is applied to charge and discharge a battery cell. This method allows for evaluating lithium stripping and plating stability by plotting potential *versus* time across varying current densities in a symmetric cell configuration (Li/SSE/Li). For full-cell assessments, the rate of charge or discharge is expressed in terms of C-rates rather than current density, as this metric indicates the time required for a battery to fully charge or discharge its capacity; for instance, a 1C rate equates to one hour, while a 10C rate corresponds to six minutes.

In the context of all-solid-state lithium batteries (ASSLBs), the lithium content within the cell dictates its theoretical capacity. The applicable current density for testing is derived from dividing the theoretical specific capacity (expressed in mA h^{-1}) by the discharge duration (in hours).

For a comprehensive understanding of a cell's research and development value at the laboratory scale, it is prudent to conduct galvanostatic cycling (GC) tests under different stack pressures, temperatures, and cathode active material (CAM) loadings, at C-rates ranging from 0.05C to 20C as shown in Fig. 6. Optimal stack pressures during battery operation should be maintained at approximately 0.1 MPa to ensure scalability; pressures exceeding 10 MPa are typically impractical for mass production. Nonetheless, to compensate for suboptimal solid component contacts, most solid-state cells undergo testing at lab scale under stack pressures above 5 MPa at its declared 'optimized pressure'.[40] The correlation of capacity fade with stack pressure is illuminating for the transition from lab-scale to prototype development. Besides stack pressure, temperature has a significant influence on battery kinetics. Furthermore, the CAM loading is crucial as it impacts the lithium diffusion coefficient through its effect on the tortuosity and porosity of the cathode, consequently affecting GC performance. Hennequart *et al.* evaluated these parameters on a halide-based $Li_3YBr_2Cl_4$ solid electrolyte, successfully operating at 0.1 MPa against a Li–In anode with minimal capacity loss from 5 MPa to 0.1 MPa under a 1C rate.[44] Substantial capacity losses were reported with increased NMC loading from 5 mg cm^{-2} to 20 mg cm^{-2} and with temperature reductions from 50 to 10 °C under a 1C rate. They determined that the hardness of the halide solid electrolyte predominantly governs GC performance, more so than its ionic conductivity.

GC provides direct information regarding capacity, energy density, and cycling stability. However, its limitation becomes obvious in that it only quantifies the cell performance but does not provide scientific justifications. For example, it lacks a way to monitor interfacial resistance. Due to poor contacts between the electrode and electrolyte in SSBs, high interfacial resistance is inevitable during cycling. This can lead to significant polarization under constant current conditions, which may obscure true material capabilities and lead to misleading interpretations of the battery's performance. Similarly, applying constant current can induce mechanical stresses within the solid components of the battery, particularly if there are mismatches in thermal and mechanical expansion between the solid electrolyte and electrode materials. These stresses can exacerbate delamination, cracking, or other mechanical degradation phenomena, which galvanostatic cycling does not inherently monitor. Lastly, GC cannot predict a battery's calendar life, which is independent of cycle numbers.

GC is an essential tool for quantifying capacity fade in batteries, predominantly due to interfacial degradation. However, the scope of GC does not extend to elucidating the chemical or structural defects at the battery's interfaces, which are critical in the capacity fade mechanism. The integration of cross-sectional Raman imaging with GC can penetrate these layers of complexity, bringing insights regarding dynamic interfacial changes. This integrated approach enables a comprehensive discourse between the quantitative facets of GC and the qualitative revelations from Raman imaging, advancing our comprehension of connection between a battery's performance and its underlying chemistry mechanisms.

After intensive GC, both cathode/SSE and anode/SSE interfaces experience degradation, which is attributed to SEI and

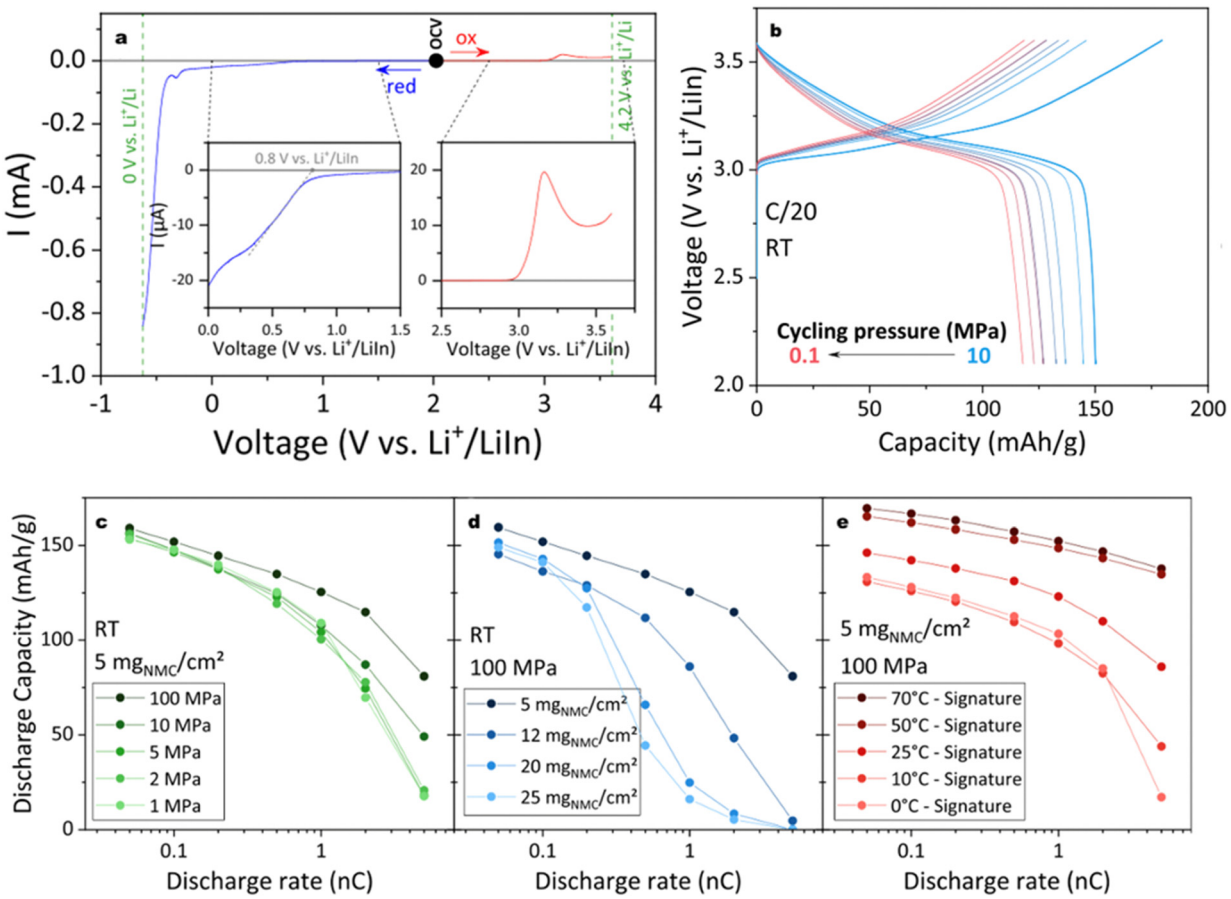

Fig. 6 (a) LSV profile with the oxidation and reduction potential of LYBC/VGCF; (b) performance of NMC//LYBC//LPSCl//LiIn as a function of stack pressure; plotted discharged capacity *versus* c rate under a certain variable: (c) stack pressure from 100 MPa to 1 MPa, (d) CAM loading from 5 to 25 mg_{NMC} cm^{-2}, (e) temperature from 70 to 0 °C. Unless noted otherwise, all cells were tested in 25 °C 100 MPa and 5 mg_{NMC} cm^{-2} as standard. Reproduced from ref. 44 with permission from American Chemical Society, copyright 2024.

cathode electrolyte interphase (CEI) passive layers. These interfaces can be explored through Raman imaging. This post cycle Raman characterization or *ex situ* Raman imaging are very common in many reports for exploring the mechanism of capacity fade.

2.4 GITT: determine the diffusion coefficient of lithium ion within the cathode

The galvanostatic intermittent titration technique (GITT) is a method for measuring the diffusion coefficient of lithium ions, which is crucial for assessing the rate capability of charge and discharge processes in batteries. Fig. 7 depicts a classical GITT plot illustrating the discharging and charging processes within a single cycle. Specifically, GITT involves applying a short pulse current, allowing for an extended relaxation period, and repeating this cycle until the battery is fully discharged or charged. The diffusion coefficient (D) is derived from these measurements as detailed by Fick's law and simplified in eqn (1)[71] with the assumption of $t \ll L^2/D$.

$$D = \frac{4}{\pi\tau}\left(\frac{m_B V_M}{S M_B}\right)^2 \cdot \left(\frac{\Delta E_s}{\Delta E_t}\right)^2$$

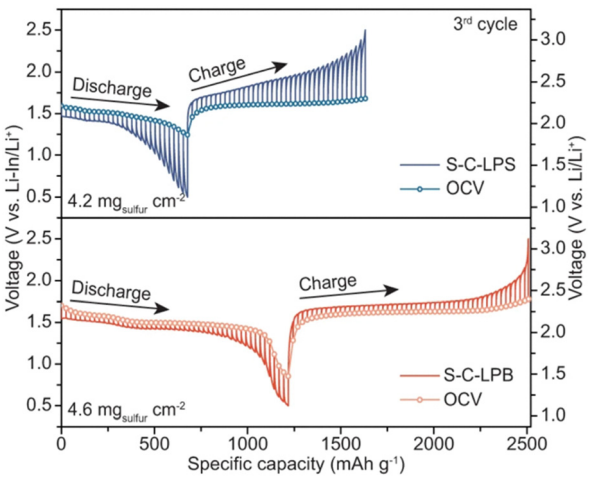

Fig. 7 Modified GITT curve for S-C-LPB and S-C-LPS cathodes using current pulses of 50.25 mA g^{-1} for 30 minutes and followed by a relaxing of 4 hours. Reproduced from ref. 72 with permission from Springer Nature, copyright 2023.

where τ is time, $\frac{m_B V_M}{M_B}$ represents the volume of active material in the electrode, $\frac{V}{S}$ is the L, the thickness of the electrode, ΔE_s is the change after the relaxation steady state process, and ΔE_t is the total voltage change for one step of GITT. Note that these simplifications are only valid if the electrode coating is free-standing, and with a high loading of active substance with minimal binders and solvents.

GITT remains a favored technique with its sole purpose of quantifying the diffusion coefficient over cyclic voltammetry (CV), which yields an average diffusion coefficient, and electrochemical impedance spectroscopy (EIS), which needs a Warburg impedance fitting model. However, GITT received many controversies of its validity due to reported discrepancies – orders of magnitude errors in the diffusion coefficients for identical materials by various research groups.[71,73]

It is necessary to meticulously select experimental conditions to satisfy the assumptions for the validity of the equations used. Kim *et al.* have provided a summary of principal experimental conditions employed by researchers,[74] highlighting the application of a low C-rate (*e.g.*, 1/20C or 1/10C) pulse for 5 to 30 minutes. The relaxation time is case-dependent, with the system reaching equilibrium typically within 1 to 10 hours. Therefore, GITT is notably time-consuming. Geng and colleagues have proposed the use of intermittent current interruption (ICI) as an alternative to GITT, citing that ICI can achieve the same diffusion coefficient results with an 85% reduction in wait time.[75] Nonetheless, the adoption of ICI remains limited within the lithium-ion battery (LIB) research community, and its reliability requires further validation by additional research groups.

Although GITT is widely employed to quantify the D value of lithium ions, it is recognized that GITT often yields apparent values that may not reflect the real diffusion coefficients. To address this discrepancy, Jia *et al.* have synergized key factors and strategies into a standard protocol for GITT that is more likely to yield the real D value.[71] They emphasize that the material's volume change during lithiation and delithiation processes can lead to inaccuracies in measurement, as indicated by the GITT equation. Based on reviewing *in situ* transmission electron microscopy (TEM) studies of silicon electrodes and associated volume expansions,[76] they propose the following guidelines: GITT is recommended if the expansion multiple (E_m) is less than 1.44; it should not be applied if E_m exceeds 2.31. For E_m values within this range, the precision of the results may be adequate for single-instance studies but is not universally applicable.

Furthermore, it is mandatory to ensure that the duration of the current pulse in the transient step of GITT is sufficiently short to satisfy the condition. Deng *et al.* established that when the ratio of t and L^2/D falls below 10%, the resultant error in the calculated diffusion coefficient (D) is negligible.[77] To meet the criterion, one could either increase the thickness of the electrode or reduce the duration of the current pulse. While minimizing pulse duration can result in tedious GITT experiments, enhancing electrode thickness proves to be a more practical solution to meet this criterion. Xu *et al.* demonstrated this approach by adjusting the thickness of a commercial electrode (SiNPs@CA@graphene oxide anode) to 82.5 μm, achieving a t to L^2/D ratio of 6.2%, thereby aligning with the established standard.[78]

While GITT provides an apparent value of lithium-ion mass transport, there remains an analytical gap regarding its application in analyzing the factors influencing lithium-ion transport within the cathode in SSBs. These factors include: (1) the oxidation stability of the CAM, (2) the uniformity of the cathode, (3) the crystallographic properties of the cathode and particle size distribution, and (4) the influence of surface treatments and catholyte interactions. Each can significantly affect the lithium-ion diffusion pathway. GITT, by measuring the apparent lithium diffusion coefficient, offers a preliminary but crucial characterization of cathode performance. Additionally, Raman spectroscopy provides a means to visualize and quantify the cathode structure and its interphase. Together, these non-destructive techniques can enhance our comprehension of the variables impacting cathode efficiency.

GITT only explored the overall lithium-ion transport quantitively in a more engineering perspective. To describe what chemicals in interphases impede the lithium migration, Raman mapping is required to visualize the chemical composition distribution inside the electrode. However, there is no report to synergize this critical connection yet.

2.5 *In situ*/*operando* Raman spectroscopy (*i-s*/*o* RS)

Traditional electrochemical methods provide comprehensive evaluations of ionic conductivity, ESW, capacity retention, and lithium diffusion coefficients. However, elucidating the causes of losses in electrochemical properties remains a significant research gap. To bridge this gap, the adoption of *in situ* diagnostic techniques is essential for real-time monitoring of volumetric and structural changes in solid electrolytes, SSE/electrode interfaces, and electrodes during electrochemical processes. *In situ*/*operando* Raman spectroscopy (*i-s*/*o* RS), favored over *in situ* XRDor TEM, offers a non-destructive alternative that does not damage the sample under investigation. This methodology avoids repeating cell assembly, thereby mitigating reproducibility issues.

Is/*o* RS is extensively employed to characterize structural and compositional changes in electrodes, SEs, and their interfaces. Li *et al.* explored the chemical stability between $Li_{10}GeP_2S_{12}$ (LGPS) and aluminum-substituted $LiNi_{0.85-x}Co_{0.15}Al_xO_2$ (with x values of 0.25, 0.15, and 0.05) utilizing EIS and *i-s*/*o* RS.[79] A 1 : 1 mass ratio of cathode material to LGPS was homogenized, pelletized, and subjected to EIS and *i-s*/*o* RS assessments. The impedance analysis indicated a relatively slower increase in resistance for the NCA(025) compared to NCA(005) in Fig. 8(a)–(d), suggesting that aluminum addition could attenuate side reactions at the cathode–SSE interface. Real-time *i-s*/*o* RS monitoring revealed the emergence and evolution of a peak at 1441 cm^{-1} for NCA(005), intensifying between 60 and 150 minutes. However, for NCA(025), a peak at 1441 cm^{-1} diminished within 120 minutes before reappearing at 150 minutes, implying that while aluminum addition mitigates interface instability, it does not entirely inhibit side

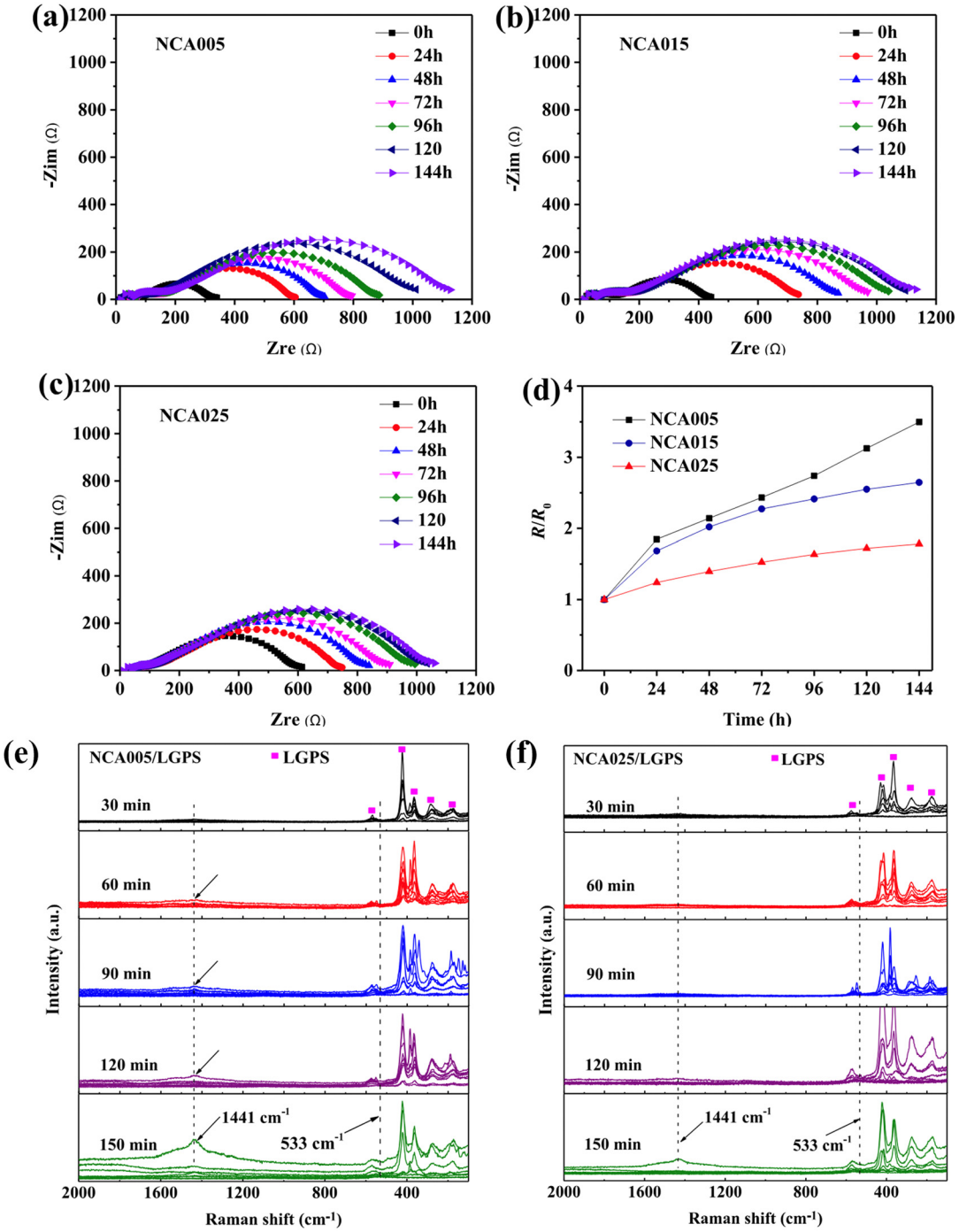

Fig. 8 (a)–(c) Nyquist plots were collected every 24 hours till 144 hours for NCA005, NCA015, and NCA025; (d) relative resistance analysis *versus* time for three cells, highlighting the magnitude of resistance evolution; (e) and (f) time resolved Raman spectra from 30 to 150 mins for NCA005 and 025, highlighting the effectiveness of Al to suppress interfacial degradation. Reproduced from ref. 79 with permission from Elsevier, copyright 2020.

reactions. However, a significant knowledge gap remains in comprehending the failure mechanisms of full cells during cycling, particularly through the application of electrochemical impedance EIS and *i-s/o* RS. Key aspects such as the expansion of interphase thickness and the evolving structural and compositional dynamics within the interphase are not fully understood. A deeper understanding of the chemistry that drives the increase in resistance is critical for identifying and addressing the primary factors that limit performance.

Lang *et al.* employed *operando* confocal Raman microscopy to elucidate the dynamic evolution of the cathode in a lithium–sulfur (Li–S) battery during galvanostatic cycling.[80] Fig. 9 correlates the galvanostatic discharging profiles with Raman spectral mapping as a function of the depth of discharge (DOD).

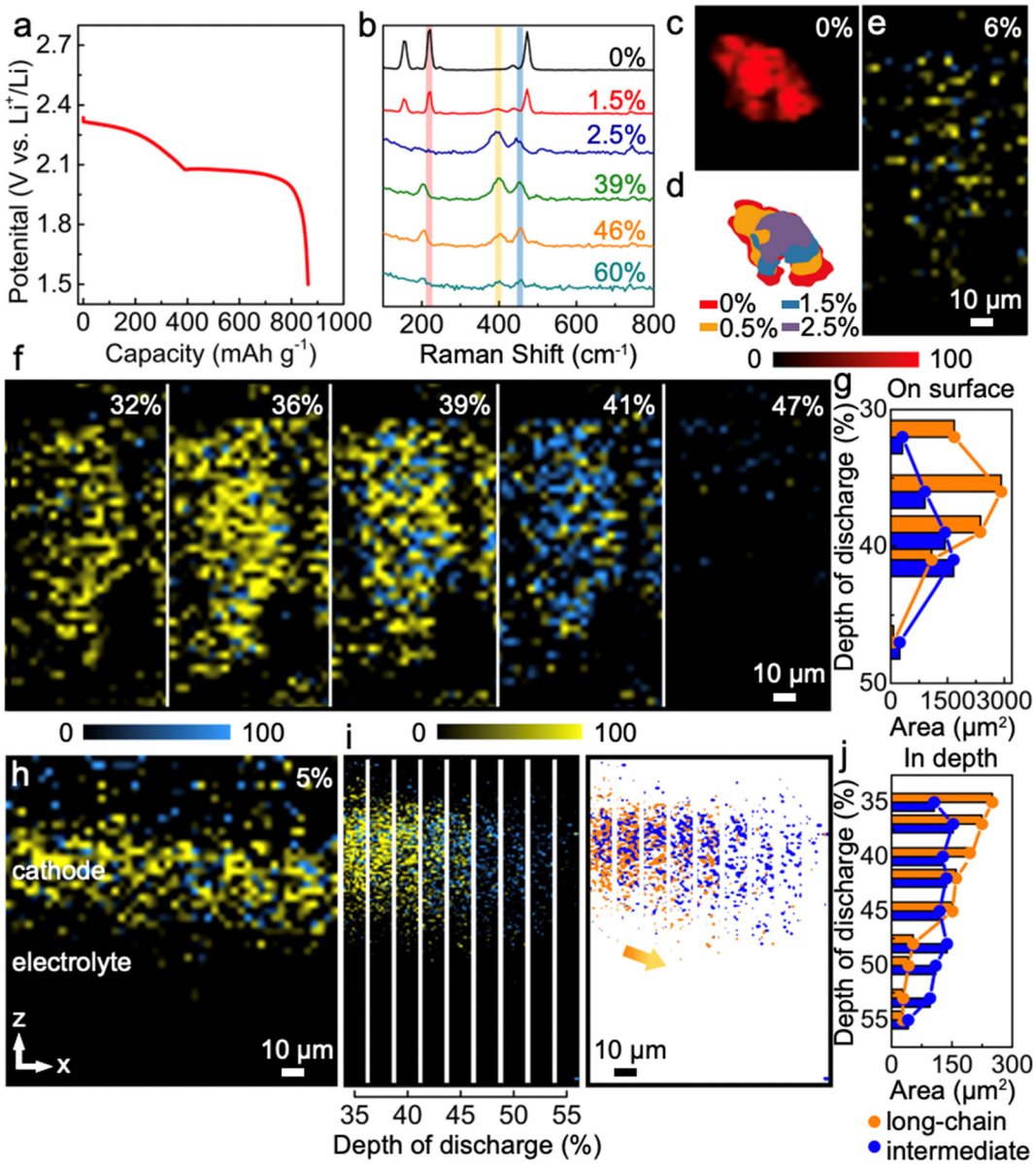

Fig. 9 Using *operando* confocal Raman to investigate Li–S redox processes. (a) Galvanostatic discharging process presented by voltage profile; (b) depth of discharge dependent Raman spectra; (c)–(g) corresponding Raman mapping results with quantified analysis; (h)–(j) depth profiling (*z*-direction) mapping images of polysulfide reactions, and its quantified analysis to highlight long-chain and intermediate. Reproduced from ref. 80 with permission from Springer Nature, copyright 2022.

This analysis provides insights into the formation and transformation of polysulfides, as well as diffusion processes, offering valuable data for identifying mechanisms of redox reaction to enhance battery performance. However, the application of time-dependent *operando* Raman spectroscopy in conjunction with galvanostatic cycling remains largely unexplored in the context of all-solid-state lithium batteries. To advance research in this area, we suggest two strategic approaches:

1. For cells with fewer than 100 cycles that present significant capacity decay, we recommend detailed examination of the initial charging and discharging cycles using *operando* RS. This early-stage analysis is crucial for understanding cathode evolution mechanisms that dictate the cell's rate capability and cycling stability.

2. For cells approaching state-of-the-art performance with more than 500 cycles, periodic Raman mapping at intervals of 100 cycles is advised to assess structural and compositional changes throughout the battery. Attention should be concentrated on the evolution of interphase thickness and composition at the electrode–solid electrolyte interfaces.

To summarize, the function and applications of Raman spectroscopy in sulfide SSBs are as follows:

1. RS can probe the interfacial structure to determine which composition is favored for facilitating Li ion mobility.

2. RS examines whether a deformation product exists when the operating potential is higher than its threshold potential.

3. RS can complement GITT analysis to strengthen evidence of the limiting factors in diffusion process in either cathode or anode.

4. *In situ* RS brings real-time insights to explore the mechanisms of limiting steps inside of the battery which strengthen battery researchers' understanding from the molecular-level to the overall performance of the cell.

However, the limitation of Raman spectroscopy falls in both hardware and large data-processing challenges. Raman spectroscopy releases scattering light which only detects Raman active material and ignores inactive material. Furthermore, interpretation of some peaks can be difficult due to convolution from peaks from two or more species. For example, in a composite NMC cathode (including LPSCl and NMC), the Raman peaks range from 200 to 300 cm^{-1}, and overlapping signals can be hard to determine which are assigned to NMC peaks[81] at around 285 cm^{-1} and Li_2CO_3 290 cm^{-1}.

In addition, the laser power must be carefully tailored if working with carbonaceous material (*e.g.* carbon black, vapor growth carbon fiber (VGCF)) to avoid burning samples. However, lowering the laser signal can result in requiring a longer accumulation time to meet better peak intensity resolution. In particular, it is important to deal with some critical compositions of material that are semi-active towards Raman scattering light.

Raman imaging also suffers from several limitations. As is well known, Raman imaging can only detect microns resolution, which is not sufficient to distill nano chemistry.[82] Additionally, a mapping size with sufficient axial points (>2000) usually takes hours to accumulate, so the transition state is hard to capture when performing *in situ* mapping. Although certain technologies have been developed, such as the 'SWIFT mode' developed by Horiba company which changes the spectral collecting mode to make the mapping speed faster, they did not help that much when the mapping spectra accumulation time is above 0.5 s. Furthermore, special data processing algorithms are needed to extract useful information from a large dataset.[83]

2.6 Evolution of electro- and chemical characterization: from an integrated to synergistic method

The integration between electro and chemical methods is commonly applied in sulfide SSEs. Cao *et al.* explored the unique electrochemical mechanisms in sulfide SSBs with sulfur conversion cathodes,[84] focusing on the solid-state reactions that influence the performance of the sulfur cathode. Electrochemical evaluations using GC and CV identified a single discharge plateau and diminished redox peak, suggesting a potentially distinct reaction pathway where S_8 directly converts to Li_2S, with Li_2S_2 serving as an intermediate in solid-state Li–S batteries. This indicates a unique polysulfide mechanism differentiating solid-state from liquid-phase systems. To corroborate this hypothesis, the integration of chemical characterization is essential to provide definitive chemical evidence.

To explore these mechanisms, the study combined *operando* Raman spectroscopy with *ex situ* X-ray absorption near-edge structure (XANES) spectroscopy. Raman spectroscopy provided real-time monitoring of the chemical evolution of the sulfur cathode during discharge, showing the gradual reduction of S_8 and the emergence of Li_2S_2. However, Raman alone could not fully justify the reaction mechanisms due to its limitations in detecting small changes in sulfur's oxidation states. This is where sulfur K-edge XANES proved crucial, offering high sensitivity to the sulfur chemical environment and confirming the presence of Li_2S and Li_2S_2, while ruling out the formation of long-chain polysulfides. Electrochemical evaluations of SSBs provide crucial performance insights but miss detailed chemical and structural changes. Raman spectroscopy and XANES fill this gap by tracking *in situ* structural transformations and offering precise chemical state analyses during operation. Integrating these spectroscopic techniques with electrochemical methods bridges the macroscopic performance metrics with microscopic material insights, enabling targeted battery design improvements and pinpointing degradation mechanisms. This comprehensive approach highlights the importance of integrating multiple characterization methods to overcome the limitations of individual techniques and achieve a thorough understanding of complex electrochemical reactions.

Nikodimos *et al.* improved the moisture robustness of LPSCl using nano-level Lewis acid additives.[85] Direct proof can be seen in the EIS Nyquist plot with effectively suppressed resistance growth after moisture exposure, and more stable cycling performance evidenced in GC. To illustrate its mechanism, XRD and *in situ* Raman spectroscopy first confirmed that the LPSCl structure remained minimally impacted after treatment, even under humid conditions. From a deeper angle, NMR and XANES spectroscopy revealed chemical interactions between the sulfur atoms and Lewis acids, evidenced by shifts in 33S NMR and sulfur L-edge XANES spectra. This provides its underlying mechanism that Lewis acid interacts with sulfur species in LPSCl, which isolates direct contamination with water. A multimodal approach provides a complete picture from its initial electrochemical evaluation to atomic explanation achieved with advanced characterization techniques.

Kim *et al.* developed a thin film sulfide SSE by mixing carboxylated nitrile-butadiene rubber (XNBR) with LPSCl.[86] LSV initially presents its wide ESW. Followed by time-resolved EIS and symmetric cell cycling, they show minimal resistance evolution and stable cycling. To characterize the chemistry after processing with XNBR and toluene, FT-IR presents peak shifts toward lower wavenumbers suggesting the formation of intermolecular bonds between LPSCl and XNBR. This indicates strong interactions between the components. To further verify the chemical and structural stability of LPSCl within the thin solid electrolyte, Raman and XRD analyses were conducted. Raman spectroscopy confirmed that the vibrational modes of PS_4^{3-} in LPSCl remained intact, indicating no significant chemical alterations. XRD analysis supported these findings, showing that the diffraction pattern of the thin film matched that of pure LPSCl, with no signs of decomposition into Li_2S. These complementary techniques were essential to confirm that the LPSCl structure and chemistry remained stable during the sheet-type SSEs fabrication and operation.

We emphasized the importance of a multimodal approach, physically applying different advanced characterization tools

with electrochemical methods in the study of sulfide SSEs. In various instances, we have explored the rationale for applying these methods in conjunction. Nonetheless, to transcend the integrated approach, greater emphasis must be placed on employing synergistic methods to characterize battery performance and underlying mechanisms comprehensively. For example, combining three-electrode EIS with *in situ* Raman spectroscopy can elucidate whether impedance at the anode or cathode interphase primarily limits performance during cycling, along with associated structural changes at these interfaces. Sole reliance on Raman spectroscopy or other chemical characterization techniques falls short of determining which cell component is the bottleneck or identifying the electrochemical factors contributing to performance degradation. In contrast, three-electrode EIS specifically pinpoints performance losses to the growth of interfacial resistance. Additionally, GITT can determine whether performance constraints are due to lithium diffusion processes in electrodes. It is crucial to integrate these non-invasive characterization techniques, particularly for the study of sulfide SSEs during cell cycling. Looking ahead, a deeper scientific understanding is anticipated through the synergized application of electrochemical and chemical characterization methods.

3. Evaluate sulfide SSBs: standardization of testing parameters

With the rapid growth of reported original research papers on solid-state batteries, most groups compare their battery performance with the parameters found in other reports. However, these interlaboratory data are usually not comparable due to unforeseen different conditions during measurements.[87] Furthermore, nontransparent reporting, due to IP concerns or simply ignoring inconsistent results, and reproducibility issues, make it difficult to benchmark performance of a 'new electrolyte', or 'new material'. Thus, it is urgent but informative to develop a standardized protocol in the field of solid-state batteries.

The meticulous reporting of material details as part of standardization testing is essential. Such reporting includes comprehensive specifics on the chemical composition, purity, particle size, morphology, and specific post-processing treatments or coatings of SSB materials (see Table 1). This depth of detail enables researchers and engineers to precisely assess the impact of these materials on battery performance, safety, and longevity. Crucially, the documentation should also cover vendor information and batch numbers, as well as detailed properties of materials, such as ionic conductivity for electrolytes and proportions of active materials, binders, and conductive additives in electrodes. This comprehensive level of transparency is vital not only for validating experimental results and facilitating comparisons across different studies but also for enhancing the scientific understanding of how these materials behave under varying operational conditions. Moreover, detailed reporting aids significantly in optimizing and developing SSBs, supporting standardized industry practices essential for commercial scalability and regulatory compliance.

Unlike conventional lithium-ion batteries with liquid electrolytes, sulfide SSBs encounter many interfacial challenges that influence the choice of processing and testing parameters during full cell evaluation.[88] Consequently, it is essential to standardize certain critical parameters. Specifically, every peer-reviewed publication in the SSB field should report the fabricating pressure and stack pressure of the cell, as SSBs require optimal contact among all cell components to guarantee satisfactory lithium-ion conductivity. Shirley Meng *et al.* investigated the fabrication pressure and stack pressure effects on electrolyte ionic conductivity and cycling performance of battery performance.[40] They

Table 1 A sample of standardized cell parameters for sulfide solid-state battery construction

Category	Parameter	Details/description
Anode	Type	Lithium metal
	Composition	99.9% pure lithium, stabilized surface (*e.g.*, LiPON coating)
	Loading level	mg cm^{-2}
	Thickness	Specified in micrometers
	Density	Specified in g cm^{-3}
Cathode	Type	NMC (nickel manganese cobalt oxide), LFP, conversion type, *etc.*
	Composition	Detailed composition, including carbon additive, binder, *etc.*
	Loading level	mg cm^{-2}
	Thickness	Specified in micrometers
	Density	Specified in g cm^{-3}
	Porosity	Percentage
	Tortuosity	
Sulfide SSE	Type	Beta-Li_3PS_4, Li_6PS_5Cl, *etc.*
	Binder content	Percentage by weight or volume
	Thickness	Specified in micrometers
	Density	Specified in g cm^{-3}
All materials	Vendor	
	Purity	Percentage
	Post-processing	Milling; calendering; sintering

Table 2 Key testing parameters for a full-cell SSB evaluation

Testing parameter	Description	Measurement level
Cell capacity or areal capacity	Total and per area capacity of the cell	mA h^{-1} or mA h cm^{-2}
C-rate	Discharge/charge rates based on theoretical capacity	C (*e.g.*, 1C, 0.5C)
Operating voltage	Range of voltage the cell operates under	Volts (V)
Pre-cycling conditions	Conditions before cycling like temperature, state of charge	Descriptive
Initial charge/discharge capacity	Capacity during the first cycle	mA h^{-1}
Coulombic efficiency	Ratio of discharge capacity to charge capacity	Percentage (%)
Energy density evaluations	Energy per unit mass or volume at different scales	W h kg^{-1}, W h L^{-1}, material, cell, pack

found increasing both the fabrication and stack pressure can significantly improve the measured ionic conductivity for pelletized LPSCl, and therefore cycling performance, because a higher fabrication pressure helps to densify the material and a higher stack pressure improves the contact between electrolyte and current collectors. To better assist standardization of pressures, we are committed to documenting both the fabrication and stack pressures used in PEEK cells in all future reports. It not only addresses the consistency and reproductivity issues, but also can define the capability of equipment and facilities from each group. For example, the Samsung team achieved the benchmark performance of an all solid-state pouch cell through warm isostatic pressing (WIP) at a fabrication pressure of 490 MPa. It is important to note that such WIP equipment may not be widely available across the research community in this field. Therefore, by openly sharing details about the fabrication pressures used, we enable researchers to gauge their ability to replicate battery performance tests accurately, even if they are not using the most optimized conditions.

It is crucial to report certain parameters during the assembly and testing phases to mitigate prevalent inconsistencies in our field as shown in Table 1. Darren H. S. Tan *et al.* investigated cycling performance dependent on cell temperature. They revealed that when lowering the cell temperature from room temperature to −20C, the cell lost two-thirds of its capacity.[89] Complementing these findings, K Minami *et al.* reported elevated processing temperature through hot pressing improves the ionic conductivity of argyrodite powder compared with cold pressing.[90] It is essential that we integrate these findings into our standardized procedures, and the proposed Table 1 is a step towards that goal.

Furthermore, the electrochemical testing protocols for sulfide SSBs have been outlined in preceding sections and encompass methods which include EIS, CV, GITT, C rate galvanostatic cycling, and long galvanostatic cycle. Full cell testing needs to be standardized, and Table 2 summarizes some of the key parameters worth reporting.

In terms of chemical evaluations, Raman measurements also provide many challenges that also need to be standardized. As of today, no unified Raman cells are available and widely used in the literature for sulfide SSE. Most Raman cells are custom and in-house made. Thus, the variety of designs result in different compromission of measurement condition for the existing defects of cell design. For example, L. Sang *et al.* designed a plane imaging Raman cell with 50 nm Au (as the cathode) to monitor the Au/SE interphase in 2017.[91] This cell is theoretically pressure controlled with screw fasten but it is not effective for use with a real cathode (usually the thickness is three or four orders of magnitude higher) due to the limitation of plane imaging. J. Zhang and his colleges successfully made a cross-sectional imaging Raman cell for *in situ* studying the LPSCl and NMC interphase during CV scans in a PEEK mold.[69] However, it is hard to tell whether the cell is pressure-controlled and capable of monitoring stack-pressure

Table 3 Key parameters for the standardization of Raman spectral measurements

Parameter category	Parameter	Details/description
Instrument details	Brand and model	(Brand), (model)
Laser details	Type	(Type of laser)
	Wavelength	(Wavelength in nm)
	Local laser power	(Power in μW)
	Spot size	(Diameter in μm)
Optical components	Objective	(Magnification and NA)
	Grating	(Lines per mm)
	Filter	(Type of filter)
	Slit	(Width in μm)
	Pinhole	(Diameter in μm)
Raman mapping	Acquisition time	(Time per point in seconds)
	Accumulation	(Number of accumulations)
	Auto focus mode	(Enabled/disabled)
	Mapping size	(Area in μm^2)
	Step size	(Distance between points in μm)

during a charging and discharging process based on the schematic of the design. Besides this, little information about sample exposure time and laser power was reported in most literature reports, although samples are very sensitive to Raman laser dose and could be damaged irreversibly without carefully optimizing the parameters. Ultimately, the Raman cell needs to perform time resolved Raman mapping to catch the heterogenous chemical change over time at different spots. To achieve this capability, we will need a unified Raman cell design that can automatically work with Raman spectroscopy systems with well controlled pressure and hopefully temperature. The system ideally will be equipped with 'fast mapping' to efficiently monitor numerous different spots (*e.g.* each sport area is 100 μm × 100 μm) in a short time (<10 min) to capture the transient chemical and structural information in different locations. This fast-mapping imaging system brings the hope to capture the transition stage during cell cycling which is invaluable to sulfide-based SSB research communities.

The key parameters listed in Table 3 need to be reported when considering standardization of the Raman spectral measurements.

In conclusion, it is of interest that this standardization is specifically for the community who works in sulfide SSE thin film research & development and their cell evaluation in PEEK mode cells. At this early stage for sulfide SSE thin film research, establishing a uniform set of standards is a strategic move that will substantially enhance future consistency and replicability across studies.

4. Conclusion

The integration of multimodal characterization techniques, particularly combining Raman spectroscopy and electrochemical methods, has proven to be pivotal in advancing our understanding of sulfide solid-state electrolytes (SSEs) and solid-state batteries (SSBs). These combined methodologies address the intricate challenges associated with the synthesis, processing, and *in situ* performance evaluation of SSEs. Utilizing tools such as in-line Raman spectroscopy, electrochemical impedance spectroscopy (EIS), and linear sweep voltammetry (LSV) allows for real-time monitoring of structural and chemical transformations, ensuring the production of high-quality SSEs. These insights are critical for optimizing synthesis and processing conditions, thereby enhancing the performance and stability of sulfide-based SSBs. This comprehensive approach not only elucidates the fundamental structure–property relationships but also informs the development of improved materials and manufacturing protocols, setting the stage for significant advancements in energy storage technology.

5. Outlook

To propel the field of sulfide SSEs and SSBs forward, future research should concentrate on the following strategic areas:

1. Innovative material design and synthesis:

- Explore new material compositions and doping strategies aimed at enhancing ionic conductivity and mechanical robustness. Develop novel synthesis methodologies that can be scaled up for industrial applications without compromising material quality.

2. Advanced *in situ* characterization techniques:

- Expand the application of advanced *in situ* and *operando* characterization methods, such as real-time Raman spectroscopy, to gain deeper insights into the dynamic processes occurring within SSEs during battery operation. This will aid in understanding ion transport mechanisms and interfacial phenomena at unprecedented resolution.

3. Computational modeling and simulation:

- Leverage state-of-the-art computational tools, including molecular dynamics (MD) and density functional theory (DFT), to predict material behaviors and guide the design of next-generation electrodes and electrolytes. This predictive capability will accelerate the identification and optimization of promising materials.

4. Standardization of testing protocols:

- Establish and adopt standardized testing protocols across the research community to ensure consistency and reproducibility in experimental results. This will facilitate more reliable comparisons and benchmarking of different studies, fostering collaborative progress.

5. Scalable and sustainable manufacturing:

- Focus on developing scalable manufacturing processes that can produce high-performance SSEs at reduced costs and with minimal environmental impact. Innovations in processing techniques will be crucial for transitioning from laboratory-scale demonstrations to commercial-scale production.

6. Commercial integration and market deployment:

- Work towards integrating these advanced technologies into commercial products, addressing challenges related to manufacturing scalability, market acceptance, and regulatory compliance. Close collaboration with industry partners will be essential to bridge the gap between research and practical application.

By addressing these critical areas, the field of sulfide-based solid-state batteries can achieve significant breakthroughs, leading to the development of safer, more efficient, and sustainable energy storage solutions. The proposed research directions are poised to unlock the full potential of sulfide SSEs, driving the next wave of innovation in energy storage technology.

Author contributions

YL and GY wrote the initial draft; ML, LC, TZ and JN wrote a few sections of the manuscript; GY provided overall guidance and performed management of research planning and execution. All authors contribute to the manuscript editing.

Data availability

All data analyzed in this review are from previously published studies, which are publicly available and cited within the text.

Detailed references to the original works are provided to facilitate access to the data.

Conflicts of interest

There are no conflicts to declare.

Acknowledgements

This research was conducted at Oak Ridge National Laboratory, managed by UT Battelle, LLC, for the U.S. Department of Energy (DOE) and is sponsored by the Office of Energy Efficiency and Renewable Energy (EERE) in the Vehicle Technologies Office (VTO) through the Advanced Battery Materials Research (BMR) Program, managed by Drs. Simon Thompson and Tien Duong. This manuscript has been authored by UT-Battelle, LLC under Contract No. DE-AC05-00OR22725 with the U.S. Department of Energy. Authors would like to acknowledge Drs. Ritu Sahore and Andrew Westover for fruitful discussions.

References

1 S. Li, Z. Yang, S.-B. Wang, M. Ye, H. He, X. Zhang, C.-W. Nan and S. Wang, Sulfide-based composite solid electrolyte films for all-solid-state batteries, *Commun. Mater.*, 2024, **5**(1), 44.
2 W. G. Suci, H. K. Aliwarga, Y. R. Azinuddin, R. B. Setyawati, K. N. R. Stulasti and A. Purwanto, Review of various sulfide electrolyte types for solid-state lithium-ion batteries, *Open Eng.*, 2022, **12**(1), 409–423.
3 M. V. Reddy, C. M. Julien, A. Mauger and K. Zaghib, Sulfide and Oxide Inorganic Solid Electrolytes for All-Solid-State Li Batteries: A Review, *Nanomaterials*, 2020, **10**(8), 1606.
4 J. Lau, R. H. DeBlock, D. M. Butts, D. S. Ashby, C. S. Choi and B. S. Dunn, Sulfide Solid Electrolytes for Lithium Battery Applications, *Adv. Energy Mater.*, 2018, **8**(27), 1800933.
5 J. Lee, T. Lee, K. Char, K. J. Kim and J. W. Choi, Issues and Advances in Scaling up Sulfide-Based All-Solid-State Batteries, *Acc. Chem. Res.*, 2021, **54**(17), 3390–3402.
6 D. Ren, L. Lu, R. Hua, G. Zhu, X. Liu, Y. Mao, X. Rui, S. Wang, B. Zhao, H. Cui, M. Yang, H. Shen, C.-Z. Zhao, L. Wang, X. He, S. Liu, Y. Hou, T. Tan, P. Wang, Y. Nitta and M. Ouyang, Challenges and opportunities of practical sulfide-based all-solid-state batteries, *eTransportation*, 2023, **18**, 100272.
7 S. Han, J. Zhao, L. Yu, L. Jingru, G. Changdong, W. Xiuli, X. Xinhui and T. Jiangping, Recent progress of sulfide electrolytes for all-solid-state lithium batteries, *Energy Mater.*, 2022, **2**(1), 200005.
8 L. Zhou, N. Minafra, W. G. Zeier and L. F. Nazar, Innovative Approaches to Li-Argyrodite Solid Electrolytes for All-Solid-State Lithium Batteries, *Acc. Chem. Res.*, 2021, **54**(12), 2717–2728.
9 Y. Nikodimos, C.-J. Huang, B. W. Taklu, W.-N. Su and B. J. Hwang, Chemical stability of sulfide solid-state electrolytes: stability toward humid air and compatibility with solvents and binders, *Energy Environ. Sci.*, 2022, **15**(3), 991–1033.
10 C. Wang, K. Adair and X. Sun, All-Solid-State Lithium Metal Batteries with Sulfide Electrolytes: Understanding Interfacial Ion and Electron Transport, *Acc. Mater. Res.*, 2022, **3**(1), 21–32.
11 Y. Zhu, X. He and Y. Mo, First principles study on electrochemical and chemical stability of solid electrolyte–electrode interfaces in all-solid-state Li-ion batteries, *J. Mater. Chem. A*, 2016, **4**(9), 3253–3266.
12 N. Kamaya, K. Homma, Y. Yamakawa, M. Hirayama, R. Kanno, M. Yonemura, T. Kamiyama, Y. Kato, S. Hama, K. Kawamoto and A. Mitsui, A lithium superionic conductor, *Nat. Mater.*, 2011, **10**(9), 682–686.
13 M. Tatsumisago and A. Hayashi, Sulfide Glass-Ceramic Electrolytes for All-Solid-State Lithium and Sodium Batteries, *Int. J. Appl. Glass Sci.*, 2014, **5**(3), 226–235.
14 Y. Kato, S. Hori, T. Saito, K. Suzuki, M. Hirayama, A. Mitsui, M. Yonemura, H. Iba and R. Kanno, High-power all-solid-state batteries using sulfide superionic conductors, *Nat. Energy*, 2016, **1**(4), 16030.
15 J. Janek and W. G. Zeier, Challenges in speeding up solid-state battery development, *Nat. Energy*, 2023, **8**(3), 230–240.
16 S. Ohno, A. Banik, G. F. Dewald, M. A. Kraft, T. Krauskopf, N. Minafra, P. Till, M. Weiss and W. G. Zeier, Materials design of ionic conductors for solid state batteries, *Progress Energy*, 2020, **2**(2), 22001.
17 A. Banik, T. Famprikis, M. Ghidiu, S. Ohno, M. A. Kraft and W. G. Zeier, On the underestimated influence of synthetic conditions in solid ionic conductors, *Chem. Sci.*, 2021, **12**(18), 6238–6263.
18 F. M. Delnick, G. Yang, E. C. Self, H. M. Meyer and J. III; Nanda, Investigation of Complex Intermediates in Solvent-Mediated Synthesis of Thiophosphate Solid-State Electrolytes, *J. Phys. Chem. C*, 2020, **124**(50), 27396–27402.
19 A. Mills, G. Yang, W.-Y. Tsai, X. C. Chen, R. L. Sacci, B. L. Armstrong, J. D. T. Hallinan and J. Nanda, Adverse Effects of Trace Non-polar Binder on Ion Transport in Free-standing Sulfide Solid Electrolyte Separators, *J. Electrochem. Soc.*, 2023, **170**(8), 080513.
20 M. B. Dixit, J.-S. Park, P. Kenesei, J. Almer and K. B. Hatzell, Status and prospect of in situ and *operando* characterization of solid-state batteries, *Energy Environ. Sci.*, 2021, **14**(9), 4672–4711.
21 Y. Morino, H. Tsukasaki and S. Mori, Microscopic Degradation Mechanism of Argyrodite-Type Sulfide at the Solid Electrolyte–Cathode Interface, *ACS Appl. Mater. Interfaces*, 2023, **15**(19), 23051–23057.
22 F. Zhao, S. Zhang, Y. Li and X. Sun, Emerging Characterization Techniques for Electrode Interfaces in Sulfide-Based All-Solid-State Lithium Batteries, *Small Struct.*, 2022, **3**(1), 2100146.
23 A. Banik, T. Famprikis, M. Ghidiu, S. Ohno, M. A. Kraft and W. G. Zeier, On the underestimated influence of synthetic conditions in solid ionic conductors, *Chem. Sci.*, 2021, **12**(18), 6238–6263.
24 C. Yu, S. Ganapathy, E. R. H. van Eck, L. van Eijck, S. Basak, Y. Liu, L. Zhang, H. W. Zandbergen and M. Wagemaker,

Revealing the relation between the structure, Li-ion conductivity and solid-state battery performance of the argyrodite Li_6PS_5Br solid electrolyte, *J. Mater. Chem. A*, 2017, **5**(40), 21178–21188.

25 T. Ozturk, E. Ertas and O. Mert, A Berzelius Reagent, Phosphorus Decasulfide (P_4S_{10}), in Organic Syntheses, *Chem. Rev.*, 2010, **110**(6), 3419–3478.

26 S. Teragawa, K. Aso, K. Tadanaga, A. Hayashi and M. Tatsumisago, Liquid-phase synthesis of a Li_3PS_4 solid electrolyte using *N*-methylformamide for all-solid-state lithium batteries, *J. Mater. Chem. A*, 2014, **2**(14), 5095–5099.

27 Y.-T. Chen, M. A. T. Marple, D. H. S. Tan, S.-Y. Ham, B. Sayahpour, W.-K. Li, H. Yang, J. B. Lee, H. J. Hah, E. A. Wu, J.-M. Doux, J. Jang, P. Ridley, A. Cronk, G. Deysher, Z. Chen and Y. S. Meng, Investigating dry room compatibility of sulfide solid-state electrolytes for scalable manufacturing, *J. Mater. Chem. A*, 2022, **10**(13), 7155–7164.

28 Y. Sun, K. Suzuki, K. Hara, S. Hori, T.-A. Yano, M. Hara, M. Hirayama and R. Kanno, Oxygen substitution effects in $Li_{10}GeP_2S_{12}$ solid electrolyte, *J. Power Sources*, 2016, **324**, 798–803.

29 D. Xie, S. Chen, Z. Zhang, J. Ren, L. Yao, L. Wu, X. Yao and X. Xu, High ion conductive Sb_2O_5-doped β-Li_3PS_4 with excellent stability against Li for all-solid-state lithium batteries, *J. Power Sources*, 2018, **389**, 140–147.

30 C. Ling, A review of the recent progress in battery informatics, *npj Comput. Mater.*, 2022, **8**(1), 33.

31 A. Mills, W.-Y. Tsai, T. Brahmbhatt, E. C. Self, B. L. Armstrong, D. T. Hallinan, J. Nanda and G. Yang, Navigating the complexities of solvent and binder selection for solution processing of sulfide solid-state electrolytes, *MRS Commun.*, 2023, **13**(6), 1063–1070.

32 X. Zhao, L. Shen, N. Zhang, J. Yang, G. Liu, J. Wu and X. Yao, Stable Binder Boosting Sulfide Solid Electrolyte Thin Membrane for All-Solid-State Lithium Batteries, *Energy Mater. Adv.*, 2024, **5**, 0074.

33 H. Muramatsu, A. Hayashi, T. Ohtomo, S. Hama and M. Tatsumisago, Structural change of Li_2S–P_2S_5 sulfide solid electrolytes in the atmosphere, *Solid State Ionics*, 2011, **182**(1), 116–119.

34 K. Oh, D. Chang, B. Lee, D.-H. Kim, G. Yoon, I. Park, B. Kim and K. Kang, Native Defects in $Li_{10}GeP_2S_{12}$ and Their Effect on Lithium Diffusion, *Chem. Mater.*, 2018, **30**(15), 4995–5004.

35 Z. Liang, Y. Xiang, K. Wang, J. Zhu, Y. Jin, H. Wang, B. Zheng, Z. Chen, M. Tao, X. Liu, Y. Wu, R. Fu, C. Wang, M. Winter and Y. Yang, Understanding the failure process of sulfide-based all-solid-state lithium batteries via *operando* nuclear magnetic resonance spectroscopy, *Nat. Commun.*, 2023, **14**(1), 259.

36 Z. Yu, S.-L. Shang, K. Ahn, D. T. Marty, R. Feng, M. H. Engelhard, Z.-K. Liu and D. Lu, Enhancing moisture stability of sulfide solid-state electrolytes by reversible amphipathic molecular coating, *ACS Appl. Mater. Interfaces*, 2022, **14**(28), 32035–32042.

37 Z. D. Hood, A. U. Mane, A. Sundar, S. Tepavcevic, P. Zapol, U. D. Eze, S. P. Adhikari, E. Lee, G. E. Sterbinsky and J. W. Elam, Multifunctional Coatings on Sulfide-Based Solid Electrolyte Powders with Enhanced Processability, Stability, and Performance for Solid-State Batteries, *Adv. Mater.*, 2023, **35**(21), 2300673.

38 D. H. S. Tan, Y. S. Meng and J. Jang, Scaling up high-energy-density sulfidic solid-state batteries: a lab-to-pilot perspective, *Joule*, 2022, **6**(8), 1755–1769.

39 Y.-G. Lee, S. Fujiki, C. Jung, N. Suzuki, N. Yashiro, R. Omoda, D.-S. Ko, T. Shiratsuchi, T. Sugimoto, S. Ryu, J. H. Ku, T. Watanabe, Y. Park, Y. Aihara, D. Im and I. T. Han, High-energy long-cycling all-solid-state lithium metal batteries enabled by silver–carbon composite anodes, *Nat. Energy*, 2020, **5**(4), 299–308.

40 J.-M. Doux, Y. Yang, D. H. Tan, H. Nguyen, E. A. Wu, X. Wang, A. Banerjee and Y. S. Meng, Pressure effects on sulfide electrolytes for all solid-state batteries, *J. Mater. Chem. A*, 2020, **8**(10), 5049–5055.

41 J. Lim, Y. Zhou, R. H. Powell, T. Ates, S. Passerini and L. J. Hardwick, Localised degradation within sulfide-based all-solid-state electrodes visualised by Raman mapping, *Chem. Commun.*, 2023, **59**(51), 7982–7985.

42 X. Randrema, I. Leteyi Mfiban, M. Soler, I. Profatilova, M. Berthault, R. Ramos, J. Lavie, E. De Vito, L. Blanc, S. Diry, S. Launois, V. Tarnopolskiy, M. Reytier, J.-F. Colin, C. Barchasz and S. Liatard, Towards a Practical Use of Sulfide Solid Electrolytes in Solid-State Batteries: Impact of Dry Room Exposure on H_2S Release and Material Properties, *Batteries Supercaps*, 2024, **7**(1), e202300380.

43 X. Li, Q. Sun, Z. Wang, D. Song, H. Zhang, X. Shi, C. Li, L. Zhang and L. Zhu, Outstanding electrochemical performances of the all-solid-state lithium battery using Ni-rich layered oxide cathode and sulfide electrolyte, *J. Power Sources*, 2020, **456**, 227997.

44 B. Hennequart, M. Platonova, R. Chometon, T. Marchandier, A. Benedetto, E. Quemin, R. Dugas, C. Lethien and J.-M. Tarascon, Atmospheric-Pressure Operation of All-Solid-State Batteries Enabled by Halide Solid Electrolyte, *ACS Energy Lett.*, 2024, 454–460.

45 M. K. Tufail, P. Zhai, W. Khokar, M. Jia, N. Zhao and X. Guo, Evaluation of solid electrolytes: development of conventional and interdisciplinary approaches, *Interdisciplinary Mater.*, 2023, **2**(4), 529–568.

46 R. Zhang, Y. Wu, Z. Chen, Y. Wang, J. Zhu and X. Zhuang, The value of in situ/*operando* Raman spectroscopy in all-solid-state Li batteries, *J. Mater. Chem. A*, 2023, **11**(36), 19195–19209.

47 R. Deivanayagam and R. Shahbazian-Yassar, Electrochemical Methods and Protocols for Characterization of Ceramic and Polymer Electrolytes for Rechargeable Batteries, *Batteries Supercaps*, 2021, **4**(4), 596–606.

48 W. Zhang, D. A. Weber, H. Weigand, T. Arlt, I. Manke, D. Schröder, R. Koerver, T. Leichtweiss, P. Hartmann, W. G. Zeier and J. R. Janek, Interfacial Processes and Influence of Composite Cathode Microstructure Controlling the Performance of All-Solid-State Lithium Batteries, *ACS Appl. Mater. Interfaces*, 2017, **9**(21), 17835–17845.

49 A. Sakuda, H. Kitaura, A. Hayashi, K. Tadanaga and M. Tatsumisago, Modification of Interface Between LiCoO[sub 2] Electrode and Li[sub 2]S–P[sub 2]S[sub 5] Solid Electrolyte Using Li[sub 2]O–SiO[sub 2] Glassy Layers, *J. Electrochem. Soc.*, 2009, **156**(1), A27.

50 Y. Li, J. Li, J. Cheng, X. Xu, L. Chen and L. Ci, Enhanced Air and Electrochemical Stability of $Li_7P_3S_{11}$-Based Solid Electrolytes Enabled by Aliovalent Substitution of SnO_2, *Adv. Mater. Interfaces*, 2021, **8**(14), 2100368.

51 A. S. Keefe, S. Buteau, I. G. Hill and J. R. Dahn, Temperature Dependent EIS Studies Separating Charge Transfer Impedance from Contact Impedance in lithium-ion Symmetric Cells, *J. Electrochem. Soc.*, 2019, **166**(14), A3272.

52 R. P. Rao, N. Sharma, V. K. Peterson and S. Adams, Formation and conductivity studies of lithium argyrodite solid electrolytes using in situ neutron diffraction, *Solid State Ionics*, 2013, **230**, 72–76.

53 N. J. J. de Klerk, I. Rosłoń and M. Wagemaker, Diffusion Mechanism of Li Argyrodite Solid Electrolytes for Li-Ion Batteries and Prediction of Optimized Halogen Doping: The Effect of Li Vacancies, Halogens, and Halogen Disorder, *Chem. Mater.*, 2016, **28**(21), 7955–7963.

54 S. H. Hwang, S. D. Seo, D. W. Kim and A. Novel, Time-Saving Synthesis Approach for Li–Argyrodite Superionic Conductor, *Adv. Sci.*, 2023, **10**(22), 2301707.

55 A. Maddu, A. S. Sulaeman, S. Tri Wahyudi and A. Rifai, Enhancing Ionic Conductivity of Carboxymethyl Cellulose-Lithium Perchlorate with Crosslinked Citric Acid as Solid Polymer Electrolytes for Lithium Polymer Batteries, *Int. J. Renewable Energy Dev.*, 2022, **11**(4), 10.

56 X. Song, W. Yu, S. Zhou, L. Zhao, A. Li, A. Wu, L. Li and H. Huang, Enhancement of Mn-doped LiPON electrolyte for higher performance of all-solid-state thin film lithium battery, *Mater. Today Phys.*, 2023, **33**, 101037.

57 Q. Zhang, T. Wei, J. Lu, C. Sun, Y. Zhou, M. Wang, Y. Liu, B. Xiao, X. Qiu and S. Xu, The effects of PVB additives in MOFs-based solid composite electrolytes for all-solid-state lithium metal batteries, *J. Electroanal. Chem.*, 2022, **926**, 116935.

58 S. Kim, J. Choi, S.-M. Bak, L. Sang, Q. Li, A. Patra and P. V. Braun, Reversible Conversion Reactions and Small First Cycle Irreversible Capacity Loss in Metal Sulfide-Based Electrodes Enabled by Solid Electrolytes, *Adv. Funct. Mater.*, 2019, **29**(27), 1901719.

59 B. Ma, Q. Jiao, Y. Zhang, C. Lin, X. Zhang, H. Ma and S. Dai, Structure promoted electrochemical behavior and chemical stability of AgI-doped solid electrolyte in sulfide glass system, *J. Am. Ceram. Soc.*, 2020, **103**(11), 6348–6355.

60 K. Seol, C. Kaliyaperumal, A. Uthayakumar, I. Yoon, G. Lee and D. Shin, Enhancing the Moisture Stability and Electrochemical Performances of Li_6PS_5Cl Solid Electrolytes through Ga Substitution, *Electrochim. Acta*, 2023, **441**, 141757.

61 D. H. S. Tan, E. A. Wu, H. Nguyen, Z. Chen, M. A. T. Marple, J.-M. Doux, X. Wang, H. Yang, A. Banerjee and Y. S. Meng, Elucidating Reversible Electrochemical Redox of Li_6PS_5Cl Solid Electrolyte, *ACS Energy Lett.*, 2019, **4**(10), 2418–2427.

62 S. Boulineau, M. Courty, J.-M. Tarascon and V. Viallet, Mechanochemical synthesis of Li-argyrodite Li_6PS_5X (X = Cl, Br, I) as sulfur-based solid electrolytes for all solid state batteries application, *Solid State Ionics*, 2012, **221**, 1–5.

63 J. Yi, D. Zhou, Y. Liang, H. Liu, H. Ni and L.-Z. Fan, Enabling high-performance all-solid-state lithium batteries with high ionic conductive sulfide-based composite solid electrolyte and ex situ artificial SEI film, *J. Energy Chem.*, 2021, **58**, 17–24.

64 S. Luo, Z. Wang, A. Fan, X. Liu, H. Wang, W. Ma, L. Zhu and X. Zhang, A high energy and power all-solid-state lithium battery enabled by modified sulfide electrolyte film, *J. Power Sources*, 2021, **485**, 229325.

65 F. Han, Y. Zhu, X. He, Y. Mo and C. Wang, Electrochemical Stability of $Li_{10}GeP_2S_{12}$ and $Li_7La_3Zr_2O_{12}$ Solid Electrolytes, *Adv. Energy Mater.*, 2016, **6**(8), 1501590.

66 E. M. Gavilán-Arriazu, M. Mercer, O. A. Pinto, O. A. Oviedo, D. Barraco, H. Hoster and E. P. M. Leiva, Numerical simulations of cyclic voltammetry for lithium-ion intercalation in nanosized systems: finiteness of diffusion versus electrode kinetics, *J. Solid State Electrochem.*, 2020, **24**, 3279–3287.

67 W. Schmickler and E. Santos, *Interfacial electrochemistry*, Springer Science & Business Media, 2010.

68 G. Yang, Y. Zhang, J.-C. Bilheux, E. Self, A. Westover, J. Chen, H. Bilheux and J. Nanda, *Tracking the Initial Capacity Loss in Solid-State Batteries using in situ Neutron Tomography and Raman Imaging*, 2023.

69 J. Zhang, C. Zheng, L. Li, Y. Xia, H. Huang, Y. Gan, C. Liang, X. He, X. Tao and W. Zhang, Unraveling the Intra and Intercycle Interfacial Evolution of Li_6PS_5Cl-Based All-Solid-State Lithium Batteries, *Adv. Energy Mater.*, 2020, **10**(4), 1903311.

70 L. Sang, K. L. Bassett, F. C. Castro, M. J. Young, L. Chen, R. T. Haasch, J. W. Elam, V. P. Dravid, R. G. Nuzzo and A. A. Gewirth, Understanding the Effect of Interlayers at the Thiophosphate Solid Electrolyte/Lithium Interface for All-Solid-State Li Batteries, *Chem. Mater.*, 2018, **30**(24), 8747–8756.

71 M. Jia, W. Zhang, X. Cai, X. Zhan, L. Hou, C. Yuan and Z. Guo, Re-understanding the galvanostatic intermittent titration technique: pitfalls in evaluation of diffusion coefficients and rational suggestions, *J. Power Sources*, 2022, **543**, 231843.

72 D. Wang, L.-J. Jhang, R. Kou, M. Liao, S. Zheng, H. Jiang, P. Shi, G.-X. Li, K. Meng and D. Wang, Realizing high-capacity all-solid-state lithium-sulfur batteries using a low-density inorganic solid-state electrolyte, *Nat. Commun.*, 2023, **14**(1), 1895.

73 I. O. Santos-Mendoza, J. Vázquez-Arenas, I. González, G. Ramos-Sánchez and C. O. Castillo-Araiza, Revisiting Electrochemical Techniques to Characterize the Solid-State Diffusion Mechanism in Lithium-Ion Batteries, *Int. J. Chem. React. Eng.*, 2018, **17**(6), DOI: **10.1515/ijcre-2018-0095**.

74 J. Kim, S. Park, S. Hwang and W.-S. Yoon, Principles and applications of galvanostatic intermittent titration technique for lithium-ion batteries, *J. Electrochem. Sci. Technol.*, 2022, **13**(1), 19–31.

75 Z. Geng, Y.-C. Chien, M. J. Lacey, T. Thiringer and D. Brandell, Validity of solid-state Li^+ diffusion coefficient

estimation by electrochemical approaches for lithium-ion batteries, *Electrochim. Acta*, 2022, **404**, 139727.

76 Z.-L. Xu, Y. Gang, M. A. Garakani, S. Abouali, J.-Q. Huang and J.-K. Kim, Carbon-coated mesoporous silicon microsphere anodes with greatly reduced volume expansion, *J. Mater. Chem. A*, 2016, **4**(16), 6098–6106.

77 C. Deng and W. Lu, Consistent diffusivity measurement between Galvanostatic Intermittent Titration Technique and Electrochemical Impedance Spectroscopy, *J. Power Sources*, 2020, **473**, 228613.

78 H. Xu, Y. Wang, R. Chen, Y. Bai, T. Li, H. Jin, J. Wang and H. Xia, A green-synthetic spiderweb-like Si@Graphene-oxide anode material with multifunctional citric acid binder for high energy-density Li-ion batteries, *Carbon*, 2020, **157**, 330–339.

79 X. Li, H. Guan, Z. Ma, M. Liang, D. Song, H. Zhang, X. Shi, C. Li, L. Jiao and L. Zhang, *In/ex situ* Raman spectra combined with EIS for observing interface reactions between Ni-rich layered oxide cathode and sulfide electrolyte, *J. Energy Chem.*, 2020, **48**, 195–202.

80 S. Lang, S.-H. Yu, X. Feng, M. R. Krumov and H. D. Abruña, Understanding the lithium–sulfur battery redox reactions via *operando* confocal Raman microscopy, *Nat. Commun.*, 2022, **13**(1), 4811.

81 M. Wood, J. Li, R. E. Ruther, Z. Du, E. C. Self, H. M. Meyer, C. Daniel, I. Belharouak and D. L. Wood, Chemical stability and long-term cell performance of low-cobalt, Ni-Rich cathodes prepared by aqueous processing for high-energy Li-ion batteries, *Energy Storage Mater.*, 2020, **24**, 188–197.

82 G. Yang, X. Li, Y. Cheng, M. Wang, D. Ma, A. P. Sokolov, S. V. Kalinin, G. M. Veith and J. Nanda, Distilling nanoscale heterogeneity of amorphous silicon using tip-enhanced Raman spectroscopy (TERS) via multiresolution manifold learning, *Nat. Commun.*, 2021, **12**(1), 578.

83 G. Yang, M. L. Lehmann, S. Zhao, B. Li, S. Ge, P.-F. Cao, F. M. Delnick, A. P. Sokolov, T. Saito and J. Nanda, Anomalously high elastic modulus of a poly(ethylene oxide)-based composite electrolyte, *Energy Storage Mater.*, 2021, **35**, 431–442.

84 D. Cao, X. Sun, F. Li, S.-M. Bak, T. Ji, M. Geiwitz, K. S. Burch, Y. Du, G. Yang and H. Zhu, Understanding Electrochemical Reaction Mechanisms of Sulfur in All-Solid-State Batteries through Operando and Theoretical Studies, *Angew. Chem., Int. Ed.*, 2023, **62**(20), e202302363.

85 Y. Nikodimos, S.-K. Jiang, S.-J. Huang, B. W. Taklu, W.-H. Huang, G. B. Desta, T. M. Tekaligne, Z. B. Muche, K. Lakshmanan, C.-Y. Chang, T. M. Hagos, K. N. Shitaw, S.-C. Yang, S.-H. Wu, W.-N. Su and B. J. Hwang, Moisture Robustness of Li_6PS_5Cl Argyrodite Sulfide Solid Electrolyte Improved by Nano-Level Treatment with Lewis Acid Additives, *ACS Energy Lett.*, 2024, **9**(4), 1844–1852.

86 S. Kim, Y. A. Chart, S. Narayanan and M. Pasta, Thin Solid Electrolyte Separators for Solid-State Lithium–Sulfur Batteries, *Nano Lett.*, 2022, **22**(24), 10176–10183.

87 N. M. Vargas-Barbosa, My cell is better than yours, *Nat. Nanotechnol.*, 2024, **19**, 419–420.

88 T. Brahmbhatt, G. Yang, E. C. Self and J. Nanda, Cathode–sulfide solid electrolyte interfacial instability: challenges and solutions, *Front. Energy Res.*, 2020, **8**, 570754.

89 D. H. S. Tan, Y.-T. Chen, H. Yang, W. Bao, B. Sreenarayanan, J.-M. Doux, W. Li, B. Lu, S.-Y. Ham, B. Sayahpour, J. Scharf, E. A. Wu, G. Deysher, H. E. Han, H. J. Hah, H. Jeong, J. B. Lee, Z. Chen and Y. S. Meng, Carbon-free high-loading silicon anodes enabled by sulfide solid electrolytes, *Science*, 2021, **373**(6562), 1494–1499.

90 K. Minami, A. Hayashi and M. Tatsumisago, Crystallization Process for Superionic $Li_7P_3S_{11}$ Glass-Ceramic Electrolytes, *J. Am. Ceram. Soc.*, 2011, **94**(6), 1779–1783.

91 L. Z. Sang, R. T. Haasch, A. A. Gewirth and R. G. Nuzzo, Evolution at the Solid Electrolyte/Gold Electrode Interface during Lithium Deposition and Stripping, *Chem. Mater.*, 2017, **29**(7), 3029–3037.